A MASH Zone Revealed: the Mafic Complex of the Sierra Valle Fértil

Barry A. Walker, Jr[1], George W. Bergantz[1]*, Juan E. Otamendi[2], Mihai N. Ducea[3] and Eber A. Cristofolini[2]

[1]Department of Earth and Space Sciences, University of Washington, Box 351310, Seattle, WA 98195, USA;
[2]Departamento de Geología, Universidad Nacional de Río Cuarto, X5804BYA, Río Cuarto, Argentina and
[3]Department of Geosciences, University of Arizona, Tucson, AZ 85721, USA

*Corresponding author. E-mail: bergantz@u.washington.edu

ABSTRACT

The Sierra Valle Fértil Complex of west–central Argentina represents a section of the Ordovician (~470 Ma) Famatinian arc and exposes a continuous, tilted crustal arc section ranging in depth from ~12 to 32 km (~4–8 kbar pressure). This arc section exposes the complete compositional architecture from ultramafic and mafic rocks to upper crustal granodiorites. Field and compositional data are presented to document the deep (~6–8 kbar) mafic complex of the Sierra Valle Fértil. The mafic complex is composed of many tens to hundreds of plutonic cumulate bodies in a complex and non-regular arrangement. There is no simple compositional, kinematic or age relationship between neighboring plutons throughout the section, as expressed by cumulate compositions, emplacement horizon, size, composition, texture or style of contact. Amphibole gabbronorites and mafic tonalites dominate, but norites, amphibole websterites, troctolites and minor anorthosites are present. Amphibole is common but always as a replacement phase, and is never observed undergoing subsequent dehydration melting. Hence there is no evidence that voluminous tonalites were produced by dehydration melting of mafic precursors. A field-based, cumulate-removal fractionation model is presented that produces the observed compositional variations in five steps. Isotopic compositions of Sr and Nd deviate significantly from primitive mantle values, indicating a crustal contribution; however, this hybridization appears to have played a minor role in the major element evolution of the mafic complex. We interpret this isotopic and elemental decoupling as a byproduct of prolonged, punctuated MASH (melting, assimilation, storage, homogenization) processes in the lower crust. Isotopes may be the only residual evidence of assimilation within the mafic zone. This requires that melt removal from the cumulates was extraordinarily efficient.

Key words: igneous petrology; crustal contamination; island arc; MASH zone; magma chamber

INTRODUCTION

There is agreement that most arc magmatism is fundamentally basaltic (Hildreth, 1981); however, the depths and specific processes whereby basalt gives rise to intermediate and silicic magmas remain in question. The dominant paradigm describing this process remains the MASH (melting, assimilation, storage, homogenization) hypothesis of Hildreth & Moorbath (1988). In this model, base-level geochemical attributes of arc magmas are established as mantle-derived basalts mix with basaltic precursors including cumulates, melt the lower crustal rocks and reside in an environment of continuing hybridization and melt removal. Numerical simulations of silicic melt generation by direct crustal melting (Bergantz, 1992; Dufek & Bergantz, 2005; Annen *et al.*, 2006) have been equivocal on the efficiency of this process, in part because they assume that assimilation is driven by simple contact melting, which is not energetically efficient (Barboza & Bergantz, 1996, 2000). Hence the possibility of intermediate magma

production occurring in lower crustal zones of anatexis rather than MASH zones, where pre-existing rock—as opposed to mantle-derived basalt—is the dominant mass contributor (Haraguchi *et al.*, 2003; Saito *et al.*, 2004, 2007; Ratajeski *et al.*, 2005; Sisson *et al.*, 2005; Clemens *et al.*, 2011; Coleman *et al.*, 2012) is controversial. Field-testing of these models has proven difficult. Numerous tilted batholiths provide cross-sectional views (Dilles, 1987; Tepper *et al.*, 1993; Bachl *et al.*, 2001; Miller & Miller, 2002; Westerman *et al.*, 2004; Kamiyama *et al.*, 2007; Walker *et al.*, 2007; Economos *et al.*, 2008; Needy *et al.*, 2009; Longo *et al.*, 2010; Putirka *et al.*, 2014; Ducea *et al.*, 2015), but most of these batholiths expose only the uppermost several kilometers of the magma system and are dominated by intermediate to evolved compositions.

The structure of deep arc crust is thus constrained by very few examples. In the absence of exposure, cognate inclusions in volcanic rocks (Conrad & Kay, 1984; Ducea & Saleeby, 1998; Lee *et al.*, 2001; Rodriguez-Vargas *et al.*, 2005; Smith, 2014; Ducea *et al.*, 2015) and seismic profiles across active arcs (Holbrook *et al.*, 1999; Yuan *et al.*, 2002; Kitamura *et al.*, 2003; Calvert *et al.*, 2008) are common proxies. Deeper exposures are often isolated blocks, beheaded and translated by faults that obscure their original position and regional context (Ross, 1985; Vernon *et al.*, 1989; DeBari, 1994; Ducea *et al.*, 2003; Kidder *et al.*, 2003; Dessimoz *et al.*, 2012; Putirka *et al.*, 2014). However, there are a few tilted sections that provide relatively continuous, mid-deep arc crust exposures on the scale of tens of kilometers: the Kohistan batholith, Pakistan (Burg *et al.*, 1998; Jagoutz *et al.*, 2007; Jagoutz, 2010); the North Cascades, USA (Miller & Paterson, 2001; Miller *et al.*, 2009); the Talkeetna arc, Alaska (DeBari & Coleman, 1989; Greene *et al.*, 2006; Rioux *et al.*, 2007; Hacker *et al.*, 2008); the Bonanza arc, Canada (Cui & Russell, 1995; DeBari *et al.*, 1999; Larocque & Canil, 2010); the Wooley Creek batholith, California (Coint *et al.*, 2013) and the Sierra Valle Fértil complex, Argentina (Otamendi *et al.*, 2009*a*; Ducea *et al.*, 2010; Tibaldi *et al.*, 2013). These field examples provide the basis for our current understanding of arc cross-sections.

In this contribution we focus primarily on the mafic complex of the Ordovician Sierra Valle Fértil (SVF) complex in northwestern Argentina, which exposes compositionally stratified, igneous arc crust interlayered with metasedimentary host-rocks at paleodepths of ∼12–32 km (Otamendi *et al.*, 2009*a*; Tibaldi *et al.*, 2013). We document the field relations, scales of compositional diversity and age relationships for a deep section within the SVF mafic zone. From our findings, several inferences arise. Although magmatism has almost completely reconstituted the crust in this arc section, the mafic zone is characterized by heterogeneity at the centimeter to kilometer scale. Gabbronorites are interlayered with tonalites in a sheet-like, but dominantly gradational and erratic fashion. Large, coherent batholiths are not present in the mafic complex. However,

this heterogeneity ends rather abruptly in the transition zone to a relatively homogeneous section of more typical arc tonalites and granodiorite batholiths that form the upper part of the section. Many of the mafic rocks do not approximate melt compositions and are interpreted to be cumulates from which evolved melt was expelled. The original textures have been variably re-equilibrated, making identification of melt-present processes difficult. Despite this, there is abundant field evidence to support a model of fractional crystallization and melt transfer combined with partial melting of the metasedimentary host-rocks for the petrogenesis of the SVF mafic complex.

GEOLOGICAL SETTING

The Famatinian Arc

The Sierra Valle Fértil (SVF) is part of the mid-Ordovician to Devonian Famatinian subduction complex that is exposed along an ∼2500 km NW–SE swath in western Bolivia and Argentina (Fig. 1). In the north (∼23°S), Famatinian arc exposures include calc-alkaline volcanic rocks, volcaniclastic rocks, sparse gabbroic mafic roots and high-level S-type plutonic rocks. The deepest Famatina exposures are between ∼28° and 33°S where the Nazca plate is currently subducting at a relatively low angle (Ducea *et al.*, 2010). The Famatinian arc represents some of the earliest subduction magmatism recognized in western South America and is interpreted to be the nascent stages of the Andean subduction system (Acenolaza *et al.*, 2002). Subduction magmatism began in the region around 550 Ma during the Pampean Orogeny (Rapela *et al.*, 1998). There was a hiatus in magmatism from ∼520 to 495 Ma. During this time unroofing of the Pampean orogen and subsequent sedimentation (Cristofolini *et al.*, 2012) created a thick (>2000 m) and widely distributed clastic sedimentary basin fill (regionally called the Puncoviscana, Suncho, Aguaditas, and Negro Peniado). Subsequently, magmatism stepped to the west. It was on and within the thick Puncoviscana sedimentary basin at the western edge of the proto-South American continent that the Famatinian arc was constructed. The arc was established at ∼495 Ma (Pankhurst *et al.*, 1998) and was active until ∼440 Ma (Collo *et al.*, 2009). In the specific vicinity of the Sierra Valle Fértil, laser ablation multicollector inductively coupled plasma mass spectrometry (LA-MC-ICP-MS) data for zircon indicate an age range of 485–465 Ma. Uranium–Pb data for zircons (chemical abrasion thermal ionization mass spectrometry; CA-TIMS), however, suggest that the initiation, operation, and death of this arc proceeded relatively rapidly—over an interval of less than 10 Myr and perhaps as little as ∼5 Myr from 472 to 467 Ma (Casquet *et al.*, 2012). Arc cessation in the south by ∼465 Ma is generally attributed to a collision with the Cuyania microplate (Thomas & Astini, 1996; Cristofolini *et al.*, 2014), but the reader is referred to the papers by Mulcahy *et al.* (2007, 2014) for further discussion.
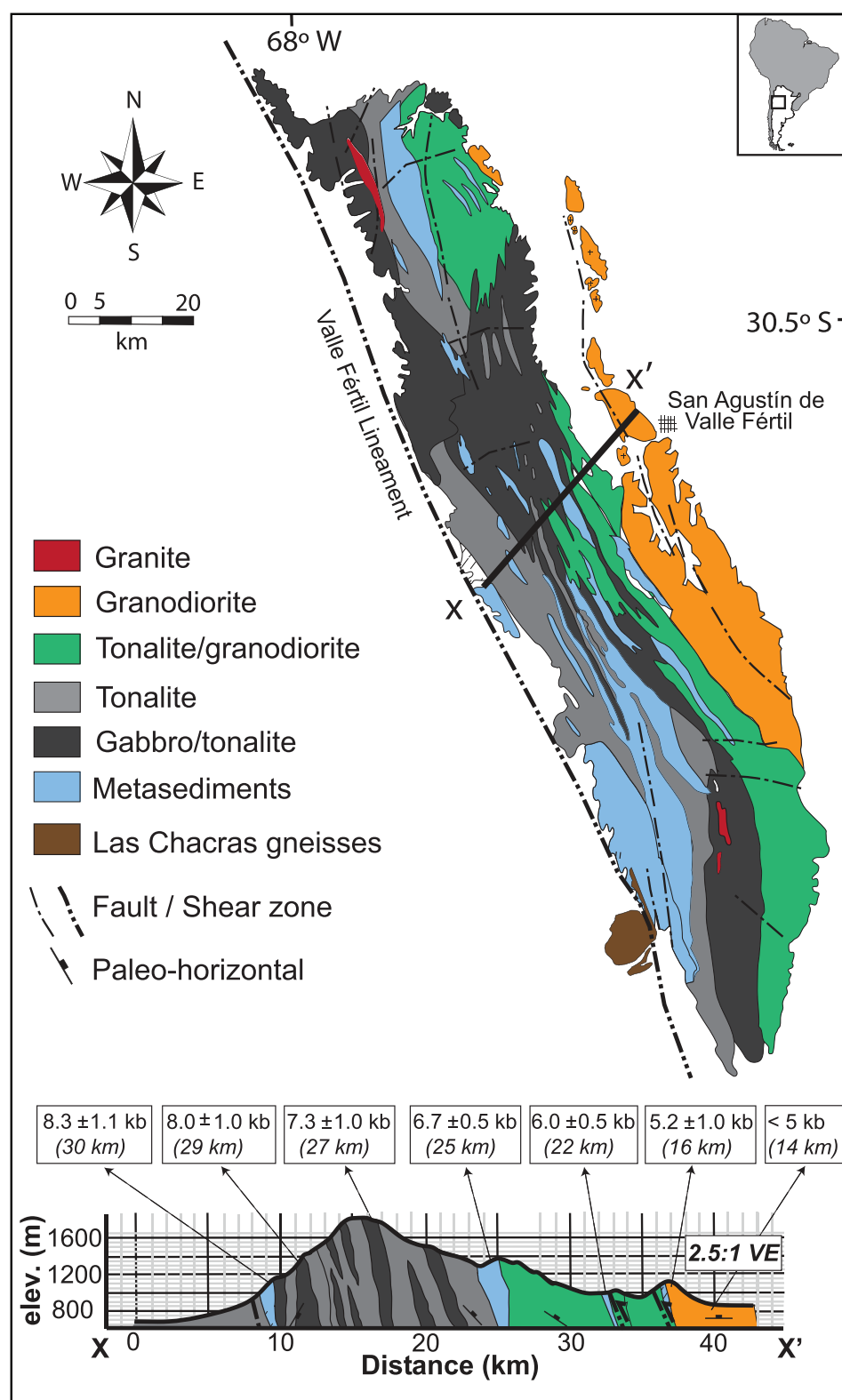
Fig. 1. Geological map of the Sierra Valle Fértil modified from the maps of Mirré (1976), Vujovich *et al.* (1996), Otamendi *et al.* (2009*b*) and Tibaldi *et al.* (2013). Cross-section and barometery modified from Tibaldi *et al.* (2013).

The Sierra Valle Fértil

The Sierra Valle Fértil is located within the southern Famatinian belt and exposes eastward-tilted arc crust from paleodepths of 12–32 km (Tibaldi *et al.*, 2013).

The SVF magmas intruded a thick, miogeoclinal sedimentary package dominated by metapelites, with minor marbles and graywackes (Cristofolini *et al.*, 2012, 2014). Otamendi *et al.* (2009*a*) have documented the vertical

distribution of distinct lithological units. From shallow to deep, the exposures include nested tonalite–granodiorite plutons that show a transition to extremely heterogeneous tonalite, which then show a transition to dominantly gabbroic and tonalitic rocks. A regional shear zone—the Valle Fértil Lineament—truncates the base of the section (Cristofolini *et al.*, 2014) (Fig. 1). Throughout the SVF screens and xenoliths of metasedimentary country rocks, ranging from centimeter to kilometer scale, are sparsely present as stromatic to diatexite migmatites. Peak metamorphism and melting of the country rocks is interpreted to have been synplutonic (Otamendi *et al.*, 2008), and interaction between metasediment-derived leucogranite melts and the SVF magmas is observable in the field. Zircon age data (Ducea *et al.*, 2010) suggest that the SVF represents a relatively brief episode towards the end of southern Famatinian magmatism (~485–465 Ma); age data from our study area suggest even shorter timescales (<6 Myr; unpublished data). This study focuses on the mafic zone of the SVF—the deeper portion of the section dominated by gabbronorite, norite, tonalite and small ultramafic bodies.

METHODS

Samples representing the compositional range of the SVF mafic zone were crushed to pea gravel size and powdered in a tungsten carbide vessel using a shatterbox. Preference was given to fresh samples without alteration. Sample sizes were typically ~0·5–1 kg of material, crushed and split. In addition to the data from previous SVF studies by Otamendi *et al.* (2008, 2009*a*, 2009*b*, 2010*a*, 2010*b*, 2012) and Ducea *et al.* (2010, 2014), 117 new whole-rock analyses are presented here.

Major and trace elements were analyzed by X-ray fluorescence (XRF, ThermoARL) at the GeoAnalytical lab at Washington State University as described by Johnson *et al.* (1999). Rare earth elements (REE) and selected trace elements were analyzed by ICP-MS (Agilent 7700, quadrupole mass spectrometer) at Washington State University. Whole-rock powders were analysed at the University of Arizona for Sr, Nd, and Pb isotopes by TIMS. Isotopic compositions were obtained using the techniques and standardization of Ducea & Saleeby (1998) and Otamendi *et al.* (2012). For several samples thin sections were analyzed using the QEMSCAN technique at the Advanced Mineralogy Research Center at the Colorado School of Mines. QEMSCAN utilizes energy-dispersive X-ray spectroscopy (EDS) to generate mineral maps of thin sections. These maps are translated into false color images from which mineral modes are calculated (Hoal *et al.*, 2009). Mineral compositions for plagioclase, amphibole, clinopyroxene, orthopyroxene, and olivine were determined at the University of Washington using a JEOL 733 electron microprobe.
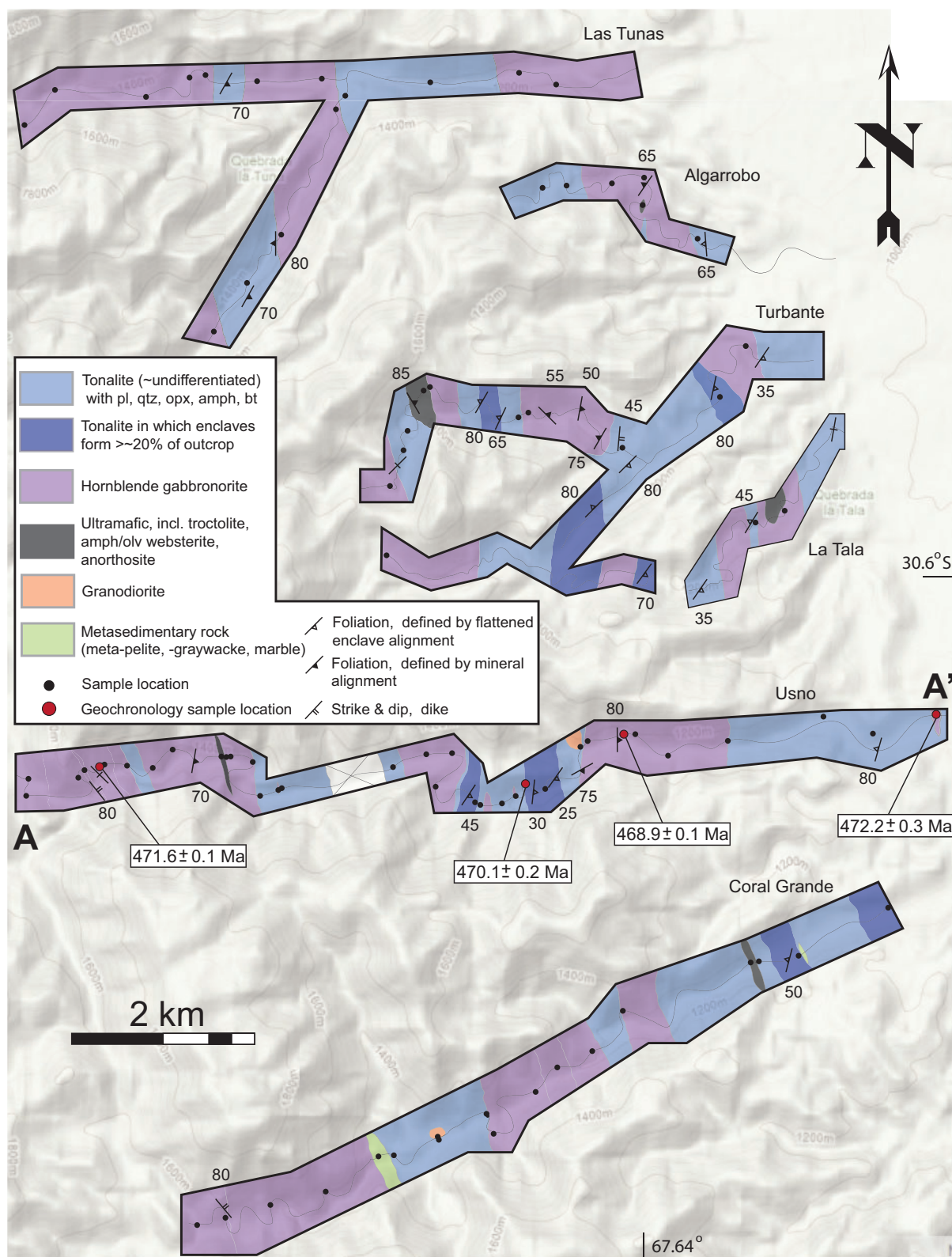
LITHOLOGICAL UNITS OF THE MAFIC ZONE

Here, we describe the rocks that form an ~100 km² area within the Valle Fértil mafic complex (Fig. 2). Exposure of fresh rock is found in several approximately east–west-oriented canyons that strike roughly perpendicular to the paleo-up direction, providing several pseudo cross-sections of the mafic zone. Outside the canyons, exposed rock is weathered, and thick vegetation prevents accurate mapping and sampling. The mafic zone section is a complex, heterogeneous assemblage of tonalite–gabbronorite, punctuated by bodies (less than kilometer scale) of ultramafic rocks, metasediments, and granite. Tonalite dominates the shallower parts of the exposed area. Within the tonalite-dominated areas, discernible gabbronorite bodies are present, although they are generally not large (~<1 km) and cannot always be inferred to extend to neighboring canyons. The gabbronorites have variable pyroxene and amphibole abundances that classify their specific rock type (e.g. gabbronorite, norite, hornblende gabbronorite), although for simplicity here we refer to these rocks as 'gabbronorites' because this is the most common variant. Contacts between the tonalite and gabbronorite bodies are usually gradational on the meter scale. Foliation and internal contacts of the tonalite and gabbronorites are typically oriented NW–SE to NE–SW and steeply dipping, consistent with the dominant foliation and map distribution of the largest bodies within the Sierra Valle Fértil complex (see Fig. 1). In places, gabbro and tonalite exposures are separated by 'transitional' zones comprising fine-grained gabbronorite with small, diffuse, stringy domains of tonalite and coarse, crystal-rich tonalite. These transitional zones have been observed to reach thicknesses of up to 30–40 m (in Usno and Turbante Canyons). Below, we discuss the tonalite and gabbronorite lithological units in more detail, as well as three other volumetrically minor units that are exposed throughout the section (see also Table 1): ultramafic cumulate rocks, fine-grained gabbroic dikes and small silicic intrusions. Highly foliated and migmatized metasedimentary host rock (cordierite/garnet biotite gneiss) is also present locally, as are cordierite-bearing diatexite domains (see Otamendi *et al.*, 2008; Tibaldi *et al.*, 2013).

Tonalite

Tonalite exposures are heterogeneous on the decimeter to meter scale with respect to modes and structures, with wispy, blob-like, and sheet-like interlayering between modally variable packages being typical (Fig. 3). Mineral foliation, defined by elongated plagioclase, biotite and amphibole, is common. Mafic sheets less than 1 m thick, inclusions, and schlieren domains are common in the tonalite and occasionally make up 20–30% of the outcrop. These inclusions typically have contacts with the host that are gradational over ~1 cm. In places, mafic inclusions appear frozen in various states of reaction or digestion, resulting in a 'ghost-like' appearance

Fig. 2. Canyon-restricted geological map of a portion of the mafic zone of the Sierra Valle Fértil complex. Boundaries of units are approximate as contacts are often gradational over ~1–40 m. The orientation of unit boundaries is based on exposures in canyons. Also shown are sample locations and specifically indicated are those samples with CA-ID-TIMS zircon dates (unpublished data). (See text for details on lithological units.)

Table 1: Petrographic descriptions of the main lithologies of the mafic zone

Lithology	Petrographic characteristics	Modes
Tonalite	Medium to coarse grained. Very heterogeneous even at thin-section scale. Inequigranular to equigranular. Plag laths or domains are subhedral but commonly comprise granophyric clusters. Qtz domains commonly have consertal texture and exhibit subgrains. Amph generally associated with opx as a rimming or reaction phase. Bio and oxides also generally associated with opx	50–60% plag (An$_{74–83}$) 10–50% qtz 0–15% opx 0–20% amph (~5% typical) 0–15% bio (<5% typical) <5% oxides trace zircon, apatite
Gabbronorite	Fine to medium grained. Relatively equigranular. Plag domains are subhedral and commonly granophyric. Cpx and opx are granular and/or blocky and usually appear clustered together. Amph usually either as a rimming or reaction phase. In some rocks, amph is observed as oikocrysts enclosing all other phases. Oxides are interstitial	50–60% plag (An$_{82–96}$) <5% qtz 15–30% opx 5–20% cpx 1–6% oxides 5–30% amph trace zircon, apatite, green spinel, pyrite
Mafic dikes	Fine grained. Plag and amph dominate and both minerals are observed as subhedral grains and grain clusters, in places with granophyric texture. Amph is, in some samples, anhedral. Oxides are interstitial, although in places they form subhedral grains	40–50% plag (An$_{95}$) 30–50% amph 0–20% opx 0–10% cpx 1–5% oxides
Relict troctolite	Medium to coarse grained. Variable mineral assemblages. Amph–plag dominant. Amph–spinel symplectite common as rims on opx. When olv is present, corona textures exist: olv–opx–amph–amph + spin–plag (see Otamendi et al., 2010). Plag commonly shows a granoblastic texture	50–60% plag ~30–40% amph 5–10% opx trace spinel, oxides, olv
Olivine–amphibole websterite	Medium grained. Olv generally heavily serpentinized. When plag is present, opx–amph–amph + spinel coronas separate it from olv. When present, amph is commonly observed as oikocrysts. Spinel occurs in symplectite with amph, and as discrete grains	10–50% olv (Fo$_{76–82}$) 10–20% cpx 10–20% opx 1–5% green spinel 0–10% plag (An$_{97–98}$) 0–25% amph

(Fig. 3b). Mafic inclusions are also observed with sharp contacts and visible reaction rims (1–2 cm wide). Metasedimentary xenoliths also occur locally. At one outcrop in Turbante canyon the tonalite unit (see Fig. 3c and d) contains blocks of metasedimentary host-rock, biotite concentrations, round quartz domains (~5 cm), large (~5 cm) cordierite crystals sheathed in biotite, plagioclase and quartz, fine-grained dark inclusions, mafic inclusions with multiple, variably coarse growth rims and ultramafic cumulate blocks (decimeter to meter scale).

The tonalite is generally medium to coarse grained (<1 cm grain size; see Fig. 4) and is dominated by plagioclase (50–60 vol. %) with variable amounts of quartz (10–50%), orthopyroxene (0–15%, but typically ~5–10%), amphibole (0–20%, but typically ~5%), biotite (0–15%, typically<5%) and Fe–Ti oxides (<5%). Zircon and apatite are observed in trace amounts. The mineral mode can be variable (quartz content in particular) over small distances (decimeters).

Gabbronorite
Gabbronorite is observed as blob-like inclusions (centimeters to meters) within the tonalite up to massive (hundreds of meters) bodies (Fig. 5). Initially subhorizontal sheets (centimeter to meter thickness) are commonly observed, but modal layering is rare. Centimeter-scale domains of tonalite are observed within the gabbronorite as patches, stringers, layers,

and occasionally dikes (centimeter to meter scale) (Fig. 5b). The gabbronorites are typically medium grained (<0·5 cm grain size), although finer grained variants are observed as inclusions. Plagioclase is the dominant mineral (~50 vol. %) and occurs as granoblastic composite grains in the form of subhedral laths. Clinopyroxene and orthopyroxene are commonly blocky and appear to be the earliest-grown phases. Plagioclase also forms blocky domains overgrown by orthopyroxene, suggesting that in some gabbronorites, orthopyroxene and plagioclase were co-crystallizing. Amphibole forms 5–30 vol. % of the gabbronorites but is rarely found as discrete, sub- to euhedral grains. Instead, amphibole is most commonly observed as rims on both clino- and orthopyroxene, and as oikocrysts ranging from ~1 to 5 cm in diameter (Fig. 5c), indicating that it crystallized late with respect to the other phases. The gabbronorites contain variable amounts of orthopyroxene (15–30%), clinopyroxene (5–20%), Fe–Ti oxides (1–5%), and quartz (<5%). Zircon, apatite, green spinel, and pyrite are observed in trace amounts. Mafic pegmatitic pods, typically centimeters to tens of centimeters in width, containing hornblende and plagioclase crystals (>1 cm), are also common (Fig. 5d).

Gabbro dikes
Fine-grained mafic dikes are observed sporadically throughout the mafic unit; these are generally several centimeters to ~1 m thick. They are dominated by
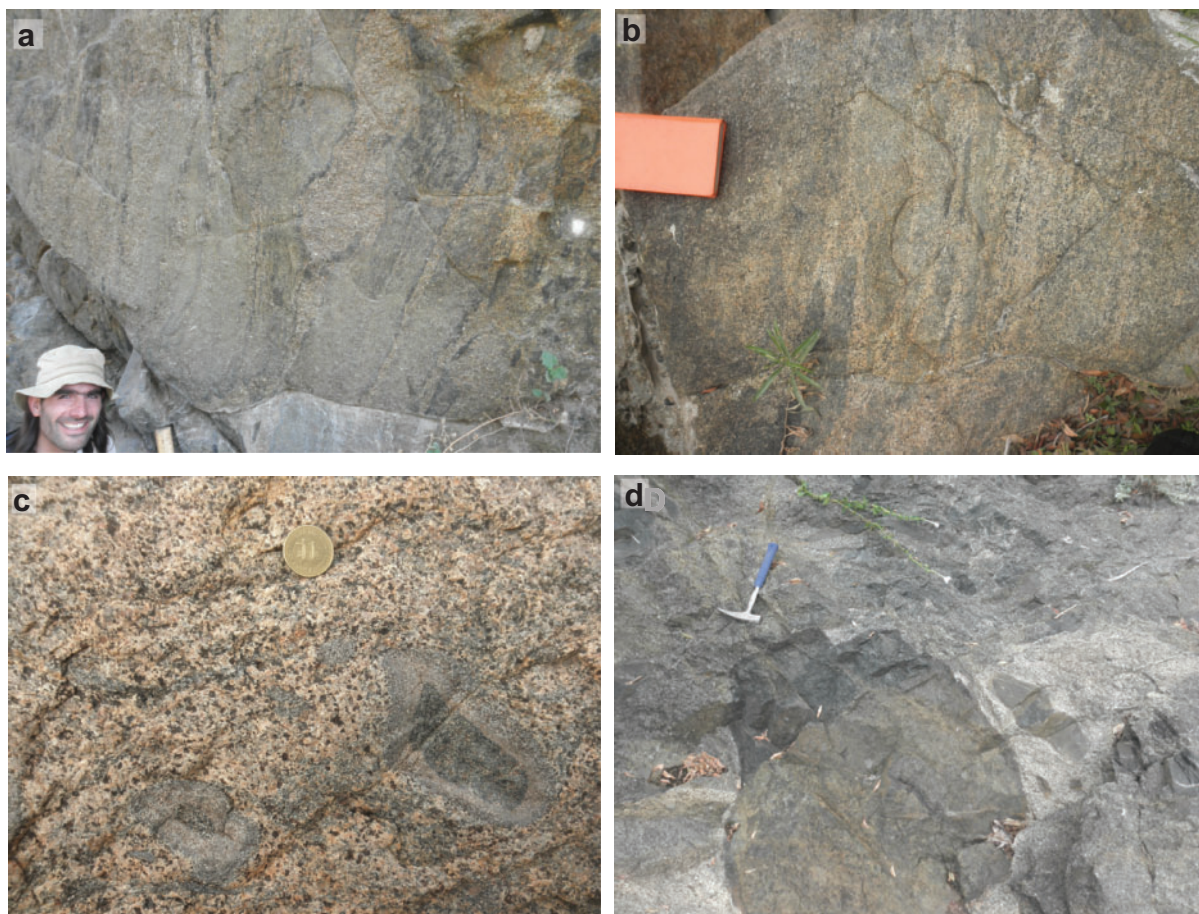
Fig. 3. Field photographs of the tonalite unit showing that it is fairly heterogeneous in outcrop. (a, b) Wispy and sheet-like interlayering with other, modally variable tonalite varieties; mafic inclusions (discrete to vestigial) are common. (c) Mafic inclusions with reaction rims in a tonalite matrix. (d) Large ~1·5 m block of olivine websterite within an inclusion-rich tonalite. Locally, blocks of other Valle Fertil rock types (metasedimentary host-rock, gabbro) are also preserved within the tonalite.

plagioclase (40–50%) and amphibole (30–50%). Unlike in the gabbronorite bodies, where amphibole is found only as rims and oikocrysts, amphibole in the mafic dikes occurs as subhedral grains and grain clusters, with triple-junction boundaries. Orthopyroxene (0–20%), clinopyroxene (0–10%) and Fe–Ti oxides (1–5%) are also present. The dikes always have sharp contacts with the host-rock.

Ultramafic bodies
The ultramafic rocks of the Valle Fértil mafic zone have been discussed in detail by Otamendi *et al.* (2010*a*), but a brief description is warranted here. They comprise clinopyroxene, orthopyroxene, olivine, amphibole, green spinel, and plagioclase. Rock types include olivine websterite, amphibole websterite, troctolite, and anorthosite. These ultramafic bodies range in thickness from tens of meters to ~400 m. They always show gradational transitions into other rock types. For the olivine and amphibole websterite bodies the transition zone is defined by an area in which plagioclase appears and then becomes dominant over an interval of ~10 m, with no sharp contact. When olivine and plagioclase are present together there is an orthopyroxene–amphibole–spinel corona

separating the two phases (Meurer & Claeson, 2002; Otamendi *et al.*, 2010*b*), suggesting partial re-equilibration in the presence of a fluid-rich phase. Amphibole is also present as rims on pyroxene and as oikocrysts, suggesting late crystallization with respect to the other phases.

Granodiorite and granite
Although rare, there are small (<0·5 km²) bodies of granodiorite and granite present in the mafic zone. We have located two 100 m size silicic blobs (Fig. 2); rare leucogranite dikes are also present. In general, granodiorite and granite are much more abundant farther up the section than in the mafic zone. These silicic rock types are noteworthy for the presence of alkali feldspar (~15–35 vol. %), which is not observed in any other rock in the mafic complex. Also present in these rock types are quartz (35–40 %), plagioclase (20–40%), and biotite (<5%).

WHOLE-ROCK COMPOSITIONS
Major and trace elements
The rocks of the Valle Fértil mafic zone range from 41 to 75% SiO$_2$ [Fig. 6; Table 2; see also Supplementary Data

Tonalite Spectrum
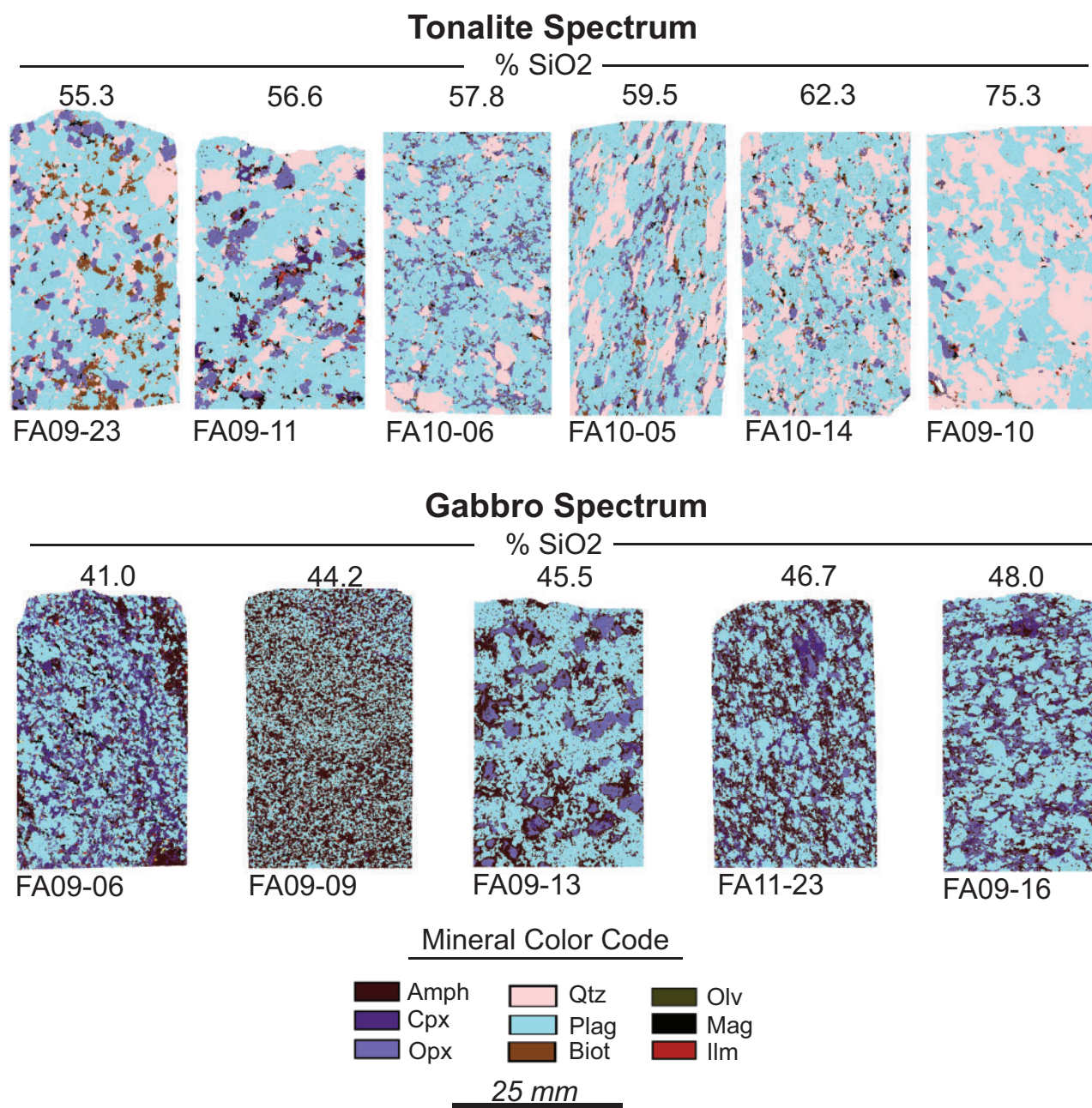
Gabbro Spectrum

Fig. 4. Selected QEMSCAN false-color photomicrographs of SVF mafic zone rocks from the tonalite and gabbronorite spectrum, with SiO_2 weight per cent indicated for each sample. Variation in the tonalite spectrum is typically in the quartz (Qtz) and orthopyroxene (Opx) content. Variation in the gabbronorite spectrum is observed in the proportions of clinopyroxene (Cpx), orthopyroxene, amphibole (Amph), and Fe–Ti oxides (Mag, Ilm). Biot, biotite; Olv, olivine; Plag, plagioclase.

(SD) Electronic Appendix 1; supplementary data are available for downloading at http://www.petrology. oxfordjournals.org]. Rocks with less than ~53% SiO_2 have compositional arrays reflecting the variable accumulation and abundance of mineral phases such as olivine, plagioclase, amphibole and Fe–Ti oxides. Specifically, olivine-bearing rocks have low TiO_2, Al_2O_3 and CaO and high MgO; plagioclase cumulates have high CaO and Al_2O_3 and low TiO_2; rocks with abundant amphibole have high TiO_2 and low SiO_2; rocks rich in Fe–Ti oxides have high FeO and TiO_2 and low SiO_2. TiO_2 and FeO are positively correlated for mafic to ultramafic

rocks. For the mafic zone rocks with >53% SiO_2 (tonalites), Al_2O_3, FeO, MgO, CaO and TiO_2 all broadly decrease with increasing SiO_2, whereas Na_2O increases with SiO_2 (up to ~62% SiO_2), consistent with a differentiation trend. With only a few exceptions, all the tonalites and gabbronorites in the mafic zone have K_2O below 1 wt % and most fall between 0·05 and 0·5 wt %.

The X_{Mg} [Mg/(Mg + Fe$_{tot}$)] of the mafic to ultramafic rocks ranges from 0·8 to 0·4. The variation of X_{Mg} versus SiO_2 is Z-shaped, with a positive correlation between X_{Mg} and SiO_2 between X_{Mg} 0·65–0·4 and SiO_2 ~50–41 wt %. The highest X_{Mg} rocks are either

Fig. 5. Field photographs of gabbro to gabbronorite, observed as massive bodies (hundreds of meters) to blob-like inclusions (centimeters) within the tonalite. (a) Wispy layering of gabbronorite varieties. (b) Tonalitic patches within the gabbronorite, which could be silicic segregations. (c) Amphibole oikocrysts, ranging in size from ~1 to 5 cm in diameter, are observed in places within the gabbronorite. (d) Typical view of the gabbronorite with silicic wisps and amphibole-rich mafic pegmatites (white arrows).

olivine-bearing or rocks that we interpret to have been originally olivine-bearing but have experienced reactive re-equilibration (relict troctolite with amphibole as the dominant mafic phase). From X_{Mg} 0·44 at SiO_2 41%, the data trend extends to higher SiO_2 with a slight decrease in X_{Mg} (0·4 to ~0·35). When the mafic and ultramafic rocks are broken out into groups with respect to their position on this X_{Mg} vs SiO_2 plot, compositional variation can be tracked in several other plots. For example, inflections are observed in TiO_2, FeO and Na_2O (all versus SiO_2).

All mafic zone rocks are enriched in incompatible trace elements with respect to primitive mantle (Sun & McDonough, 1989; Fig. 7; Table 2). Overall, negative spikes in the high field strength elements Nb, Ta, Th and U are observed in primitive mantle-normalized trace element patterns, consistent with a subduction signature. For the mafic to ultramafic rocks the abundances of trace elements are consistent with mineral modes. For the tonalites, variation with silica is consistent with the trace element's compatibility in gabbroic mineral phases (Fig. 8). For example, olivine-bearing rocks are enriched in Ni and Cr (>400 ppm and

>500 ppm respectively); Ni and Cr decrease with increasing SiO_2 in tonalites; rocks rich in clinopyroxene and Fe–Ti oxides have elevated Sc and V (>30 and >250, respectively), whereas Sc and V decrease with increasing SiO_2 in tonalites. Most mafic zone rocks (tonalites included) have extremely low concentrations of Rb and Ba (mostly <25 ppm and <200 ppm, respectively) in keeping with the low K_2O of these rocks. However, a few intermediate samples are more enriched in incompatible large ion lithophile elements such as Rb, Ba and Sr. Mafic zone rocks have REE concentrations that are enriched ~1 to 100 times relative to primitive mantle (Fig. 7). With decreasing X_{Mg}, the mafic–ultramafic rocks become more enriched in the REE. With the exception of some high-SiO_2 leucogranites, intermediate to silicic rocks from the mafic zone have Zr/Hf close to 40, consistent with chondritic and globally observed values (Hoskin & Schaltegger, 2003; Claiborne *et al.*, 2006). Most mafic to ultramafic rocks have Zr/Hf ranging from 22 to 38, suggesting some fractionation mechanism. The Eu/Eu* values for mafic–ultramafic rocks vary from 0·5 to 2·2, although most samples fall between ~0·7 and 1·5. The Eu/Eu* for more
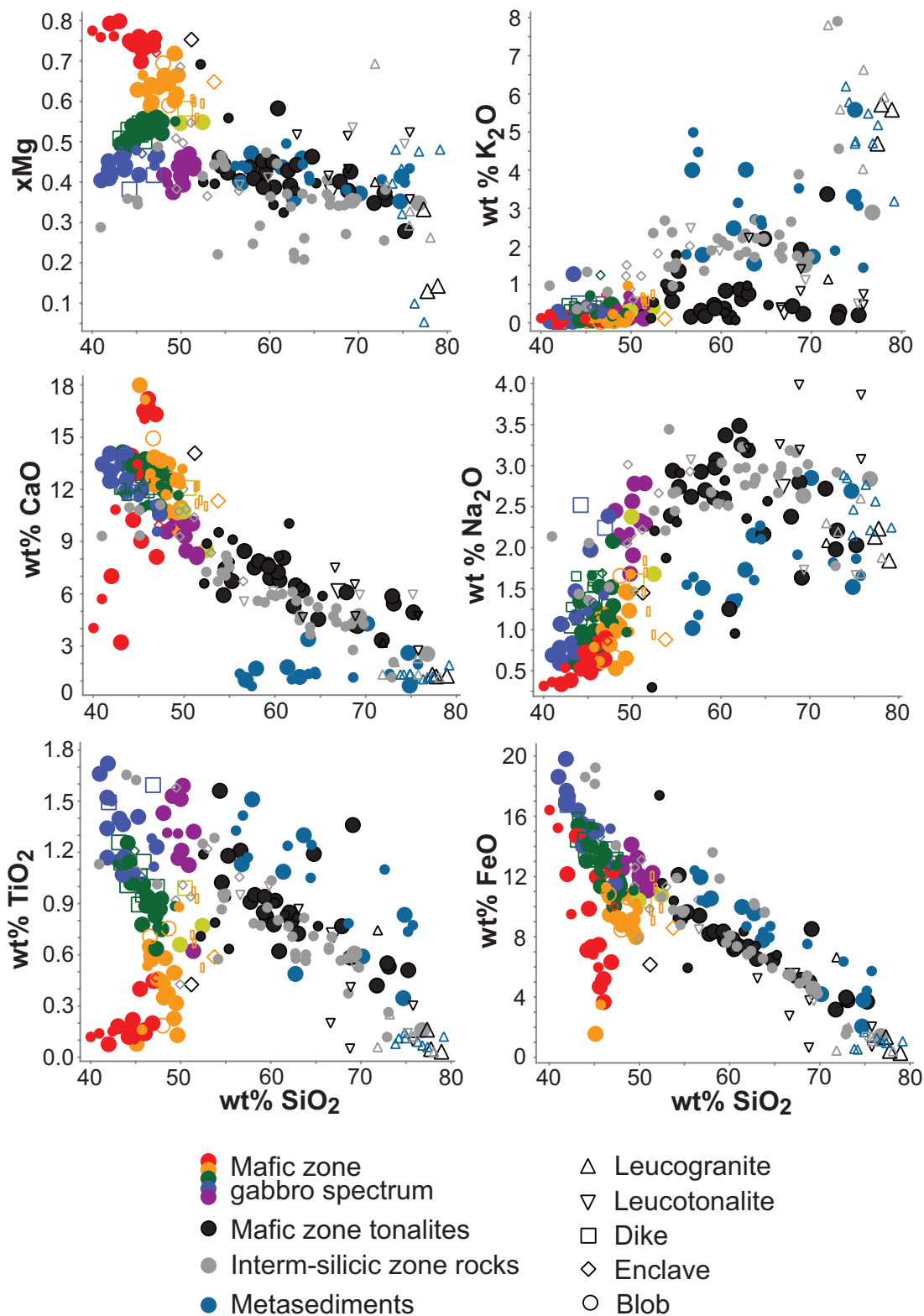
Fig. 6. Major element variations vs SiO₂ (wt %) for the SVF. The gabbroic rocks of the mafic zone rocks are color-coded based on their position in the X_{Mg} [Mg/(Mg + Fe$_{tot}$)] vs SiO₂ plot. Tonalites of the mafic zone are shown in black. Rocks from the intermediate and silicic zones are colored gray; metasedimentary rocks are colored blue. Various other rock types (dike, enclave, blob, leucogranite, leucotonalite) are identified by separate symbols. Large symbols are data from this study, and smaller symbols are data from previous studies (Otamendi *et al.*, 2008, 2009*b*, 2010*a*, 2010*b*, 2012).

Table 2: Major and trace element compositions of selected samples from the SVF mafic zone

Sample:	FA906	FA907	FA909	FA914	FA916	FA918	FA1012
Lithology:	hbl gn	qtz-gabbro	hbl-gabbro enclave	qtz-norite	hbl gn	qtz-gabbro	gn
Canyon:	Usno	Usno	Usno	Usno	Usno	Usno	Las Tunas
SiO_2	41·02	49·11	44·19	50·24	48·04	52·42	43·20
TiO_2	1·66	1·53	2·01	1·59	0·43	0·77	1·397
Al_2O_3	17·16	17·23	17·41	19·81	19·73	17·71	16·51
FeO_t	18·62	14·12	15·29	11·82	8·79	10·77	16·38
MgO	7·09	4·75	5·29	4·3	8·89	7·33	7·78
CaO	13·45	10·46	11·82	8·48	12·82	8·51	13·48
Na_2O	0·69	2·12	2·52	2·78	0·98	1·68	0·83
K_2O	0·04	0·09	0·51	0·44	0·13	0·39	0·09
Total*	97·54	99·42	98·68	98·94	98·41	99·17	98·20
X_{Mg}	0·40	0·37	0·38	0·39	0·64	0·55	0·46
Ni	22·7	21	9·1	30·2	65·4	73·7	24·6
Cr	4·7	19·2	0	54·3	250·6	253·6	72·7
Sc	62·4	45·0	60·2	30·1	38·6	38·2	60·2
V	597·4	343	332·8	235·9	227·9	302·4	541·0
Ba	14	49	115	213	46	121	36·1
Rb	0·2	0·2	1·9	5·3	0·7	8·5	0·4
Sr	159	269	259	249	195	141	185
Zr	13	231	617	467	18	73	15
Y	8·84	35·92	52·47	16·28	8·70	24·71	11·20
La	2·02	18·00	23·64	16·89	4·40	24·12	3·10
Ce	5·40	48·13	60·71	35·06	9·99	49·70	7·82
Pr	0·82	7·10	8·94	4·44	1·36	5·92	1·16
Nd	3·97	32·48	41·96	18·53	5·96	23·29	5·62
Sm	1·25	7·85	11·07	3·97	1·57	5·07	1·75
Eu	0·46	2·02	2·85	1·64	0·51	1·24	0·67
Gd	1·46	7·36	11·40	3·71	1·58	4·65	2·06
Tb	0·26	1·21	1·83	0·56	0·28	0·75	0·35
Dy	1·79	7·31	10·88	3·28	1·81	4·68	2·31
Ho	0·35	1·45	2·18	0·66	0·36	0·96	0·48
Er	1·01	3·94	5·81	1·82	0·99	2·75	1·27
Tm	0·14	0·54	0·80	0·26	0·14	0·43	0·18
Yb	0·86	3·26	4·60	1·64	0·89	2·83	1·12
Lu	0·14	0·51	0·72	0·28	0·14	0·46	0·17
U	0·01	0·08	0·40	0·27	0·03	0·61	0·05
Th	0·04	0·11	1·41	0·42	0·12	4·94	0·23
Hf	0·49	5·40	13·26	11·48	0·59	2·24	0·51

(continued)

silicic rocks is much more variable; tonalites range from 0·5 to 4·1, and leucogranites range from 2·4 to extreme values of 10·5. In general, elemental trends for the mafic to ultramafic rocks appear to reflect mineral accumulation, whereas the trends for the tonalitic rocks tend to be more linear.

Sr, Nd and Pb isotopes

The rocks of the Valle Fértil mafic zone exhibit a wide range in isotopic composition (Fig. 9; Table 3); Sr, Nd, and Pb isotope ratios fall within the Valle Fértil array reported by Otamendi *et al.* (2009*a*, 2012) and Ducea *et al.* (2014). With respect to Sr and Nd isotopes, the most remarkable characteristic of the SVF rocks is that they all deviate strongly from primitive mantle isotopic values. Within the mafic zone, initial $^{87}Sr/^{86}Sr$ (age corrected to 475 Ma) ranges from 0·70525 to 0·71445, with the mafic to ultramafic rocks spanning the entire range. Tonalites in the mafic zone are more restricted in $^{87}Sr/^{86}Sr$, ranging from 0·707531 to 0·712642 (when leucotonalite veins are excluded, the range is even more restricted at 0·709281–0·710635). Initial ε_{Nd} ranges from 2·2 to –6·5

(corresponding to a range in initial $^{143}Nd/^{144}Nd$ of 0·512137–0·511696). As for Sr isotopes, the mafic and ultramafic rocks also have the largest range in ε_{Nd} (2·2 to –5·9). Tonalites are restricted to ε_{Nd} values of –5·2 to –6·5 (with one leucotonalite vein with $\varepsilon_{Nd} = -2·5$). A negatively correlated array is observed when ε_{Nd} is plotted against $^{87}Sr/^{86}Sr$; however, variation to the highest $^{87}Sr/^{86}Sr$ values (>0·711) is associated with no systematic change in ε_{Nd} values. The samples with the highest ε_{Nd} and lowest $^{87}Sr/^{86}Sr$ have between 47·5 and 51·5 wt % SiO_2; with the exception of these rocks the mafic zone rocks show generally positive correlations in SiO_2 vs $^{87}Sr/^{86}Sr$ and negative correlations in SiO_2 vs ε_{Nd}.

Lead isotope compositions (age corrected) in the Valle Fértil mafic zone rocks show only minor variation (Table 3); $^{208}Pb/^{204}Pb$ ranges from 38·1487 to 38·5526; $^{207}Pb/^{204}Pb$ ranges from 15·6490 to 15·6606 and $^{206}Pb/^{204}Pb$ ranges from 18·2749 to 18·7270. The values reported here fall within the range of Pb isotopic compositions reported by Otamendi *et al.* (2012) for the Valle Fértil complex.

Table 2: Continued

Sample:	FA2-11-02	FA2-11-10	FA2-11-12	FA2-11-14	FA2-11-18	FA2-11-22	FA-12-01
Lithology:	hbl gn	hbl gn dike	hbl gn	gabbro enclave	gabbro	hbl gn dike	hbl gn
Canyon:	Usno	Usno	Usno	Coral Grande	Las Tunas	Coral Grande	Turbante
SiO_2	50·89	43·16	44·51	51·18	41·92	44·07	47·33
TiO_2	1·126	1·258	1·020	0·426	1·720	1·007	1·231
Al_2O_3	18·46	18·84	16·34	15·87	16·90	17·75	20·57
FeO_t	11·07	14·44	14·08	6·16	17·69	13·70	11·52
MgO	5·49	8·36	9·25	10·50	6·87	8·65	5·62
CaO	10·03	12·14	13·65	14·08	13·05	13·20	10·57
Na_2O	2·32	1·05	0·79	1·45	1·07	1·15	2·39
K_2O	0·19	0·44	0·08	0·17	0·29	0·23	0·10
Total*	99·42	97·68	99·05	98·30	96·86	97·31	99·36
X_{Mg}	0·47	0·51	0·54	0·75	0·41	0·53	0·46
Ni	32	97	53	187	34	64	22
Cr	53	106	68	1339	11	116	38
Sc	42·5	48·7	59·4	38·8	61·2	49·4	31·8
V	296	445	479	168	670	430	282
Ba	101	96	19	63	75	33	78
Rb	1·4	6·3	0·3	1·1	2·9	2·2	0·3
Sr	209	1698	175	95	219	174	277
Zr	88	17	16	28	32	16	28
Y	24·80	12·04	10·94	16·99	21·65	12·48	13·55
La	11·36	6·20	2·92	7·72	8·92	2·42	10·77
Ce	25·87	15·34	8·34	18·46	23·90	6·97	23·05
Pr	3·66	2·08	1·29	2·37	3·50	1·13	3·13
Nd	17·10	9·21	6·24	9·65	15·84	5·81	14·10
Sm	4·78	2·44	1·85	2·40	4·15	1·86	3·35
Eu	1·44	0·85	0·64	0·64	1·07	0·64	1·39
Gd	4·98	2·51	2·08	2·68	4·16	2·11	3·31
Tb	0·84	0·41	0·36	0·48	0·70	0·38	0·51
Dy	5·13	2·55	2·26	3·12	4·28	2·45	2·89
Ho	1·05	0·51	0·47	0·66	0·88	0·53	0·57
Er	2·71	1·35	1·24	1·84	2·39	1·40	1·47
Tm	0·38	0·19	0·18	0·28	0·34	0·21	0·20
Yb	2·27	1·19	1·09	1·72	2·10	1·21	1·20
Lu	0·34	0·19	0·16	0·27	0·32	0·19	0·19
U	0·06	0·12	0·01	0·17	0·04	0·05	0·03
Th	0·12	0·19	0·03	0·59	0·04	0·21	0·16
Hf	2·21	0·64	0·57	1·03	1·04	0·63	0·78

(continued)

MINERAL COMPOSITIONS OF THE MAFIC ZONE ROCKS

Olivine

Olivine occurs exclusively in the ultramafic bodies. It typically forms subhedral grains partially reacted to serpentine (Fig. 10). X_{Mg} of olivine ranges from 0·76 to 0·82, with less than 1% variation within samples (Table 4). NiO contents of olivine range from 0·07 to 0·27 wt % with ~0·05 wt % variation within samples. No zoning is observed within grains nor is there significant chemical variation within samples. This is consistent with olivine compositional variations from SVF ultramafic bodies higher in the section reported by Otamendi *et al.* (2010*a*).

Clinopyroxene

Clinopyroxene is present in ultramafic bodies, gabbronorites, and some tonalites. It typically occurs as subhedral grains (Fig. 10), although a granoblastic texture is present in places, suggesting some recrystallization. Clinopyroxene is commonly rimmed by amphibole.

Clinopyroxene X_{Mg} [Mg/(Mg + Fe$_{tot}$)] ranges from 0·67 to 0·85 [0·72–0·89 for X_{Mg} = Mg/(Mg + Fe^{2+})], with <8% variation within samples (Table 5). Clinopyroxenes from an olivine-bearing cumulate body have the highest X_{Mg}, ranging from 0·83 to 0·85, consistent with data reported by Otamendi *et al.* (2010*a*); Al_2O_3 contents of clinopyroxenes vary from 1·5 to 4·2 wt %. For each sample, there is a negative correlation between Al_2O_3 and X_{Mg} (SD Electronic Appendix Fig. 1). This trend is similar to that shown by cpx in gabbronorites from the Chilas complex (Jagoutz *et al.*, 2007), where it was explained as a metamorphic trend owing to a Tschermak exchange of (Fe,Mg)SiAl$_2$ during cooling. A similar, but less well-defined, negative correlation also exists between X_{Mg} and Na_2O for these samples. Every rim analysis of cpx from sample FA2-11-12 has a slightly higher X_{Mg} than the corresponding grain interior (X_{Mg} of ~0·77 vs 0·73–0·75).

Orthopyroxene

Orthopyroxene is observed in ultramafic bodies, gabbronorites and many tonalites. It is typically subhedral

Table 2: Continued

Sample: Lithology: Canyon:	FA911 tonalite Usno	FA912 tonalite Usno	FA1005 tonalite Usno	FA1019 tonalite Usno	FA11-12 qtz-tonalite Coral Grande	FA1014 tonalite Las Tunas	FA-12-09 tonalite Turbante	FA-12-03 tonalite Turbante
SiO_2	56·64	72·93	59·48	60·93	69·10	62·30	58·22	63·02
TiO_2	1·21	0·55	0·824	0·621	1·360	0·799	0·950	0·724
Al_2O_3	17·49	13·09	17·88	15·55	11·33	16·58	18·06	16·36
FeO_t	9·4	3·97	7·82	7·41	8·52	7·06	8·35	6·54
MgO	3·56	1·33	3·24	5·80	3·54	2·55	3·24	2·91
CaO	8·46	5·86	6·91	8·06	4·16	6·49	7·87	6·20
Na_2O	2·62	1·98	3·07	1·25	1·63	3·25	2·70	3·19
K_2O	0·16	0·14	0·40	0·15	0·23	0·62	0·18	0·75
Total*	99·27	98·82	99·13	98·74	99·43	99·32	99·19	99·79
X_{Mg}	0·40	0·37	0·42	0·58	0·43	0·39	0·41	0·44
Ni	14·8	3·7	19·3	60·5	47	10·5	14	16
Cr	18·8	7·5	34·2	219·6	107	19·1	22	26
Sc	27·1	11·4	25·5	33·6	24	22·6	26·0	18·9
V	232·7	93·3	176·3	206·4	186	147·9	175	156
Ba	82	67	141·4	64·5	138	240·0	113	519
Rb	1·0	0·8	2·9	1·3	2·7	4·3	0·8	8·9
Sr	249	184	217	140	168	207	267	178
Zr	260	78	160	41	693	151	84	118
Y	14·76	8·73	14·44	22·62	3·74	18·05	9·96	7·94
La	10·16	7·78	14·15	12·96	22·98	18·48	13·31	17·41
Ce	22·77	16·81	25·93	28·72	36·97	36·87	25·44	29·28
Pr	3·12	2·15	3·13	3·76	3·66	4·47	3·08	3·23
Nd	14·03	8·68	13·47	15·79	12·21	18·03	12·75	12·03
Sm	3·37	1·84	3·03	4·09	1·49	4·02	2·58	2·22
Eu	1·44	1·03	1·94	0·99	1·56	1·52	1·44	1·25
Gd	3·35	1·71	3·02	4·10	0·92	3·84	2·41	2·00
Tb	0·51	0·28	0·46	0·72	0·11	0·60	0·35	0·29
Dy	3·06	1·70	2·80	4·59	0·65	3·55	2·00	1·67
Ho	0·59	0·34	0·60	0·93	0·15	0·71	0·40	0·33
Er	1·63	0·98	1·69	2·57	0·51	1·90	1·04	0·87
Tm	0·23	0·15	0·26	0·37	0·10	0·27	0·14	0·12
Yb	1·36	0·92	1·80	2·30	0·89	1·74	0·88	0·81
Lu	0·23	0·15	0·30	0·35	0·17	0·27	0·14	0·14
U	0·15	0·16	0·17	0·17	0·30	0·24	0·05	0·19
Th	0·22	0·18	0·20	0·94	0·40	0·40	0·11	0·38
Hf	6·15	2·14	4·04	1·24	17·36	3·82	1·97	3·06

(continued)

and commonly rimmed by amphibole (Fig. 10). Compositionally, orthopyroxene varies in X_{Mg} from 0·57 to 0·67 (Table 6) and falls within the hypersthene field (En 55–82). Within single samples, X_{Mg} variation is <3%. In contrast to those from cumulate bodies (see Otamendi *et al.*, 2010), orthopyroxenes from the gabbronorites and tonalites of the mafic zone have significantly lower X_{Mg} (0·59–0·67 vs ∼0·81; see SD Electronic Appendix Fig. 1). These compositions fall within the field of arc 'cumulate' orthopyroxene (Spandler *et al.*, 2003).

Amphibole
Amphibole occurs most commonly (Fig. 10) as rims on pyroxene, and as oikocrysts (ranging in size from ∼1 to 5 cm in diameter). It is the dominant mafic mineral in gabbroic dikes. Compositionally, the amphiboles straddle the border of the hornblende–tschermakite–pargasite field in the classification scheme of Leake *et al.* (1997) (Table 7; SD Electronic Appendix Fig. 2). Amphibole X_{Mg} (Fe as Fe^{2+}) ranges from 0·67 to 0·83, although three samples have very similar ranges (∼0·73–0·81), whereas amphibole from FA2-11-02—a fairly deep

(∼8 kbar) gabbronorite—has an overall lower X_{Mg} (0·67–0·73, with two analyses at 0·78 and 0·81). Other than sample FA2-11-02, the observed compositional variation is minimal within samples.

Plagioclase
Plagioclase has the largest mode and is absent only in some olivine-bearing rock types. It typically comprises domains (<1 cm) of many subgrains (Fig. 10) with some granoblastic triple-point boundaries. Plagioclase anorthite contents vary from 74 to 98% (Table 8; SD Electronic Appendix Fig. 3). However, variation is minimal within samples. Plagioclase from an olivine-bearing pyroxenite (FA-09-17) has a composition of $An_{97–98}$. Three gabbronorite samples (FA-09-16, FA-09-06, and FA2-11-02) have plagioclase with $An_{95–96}$, $An_{95–96}$, and $An_{82–89}$, respectively; plagioclase from a mafic dike (FA2-11-10) is $An_{95–96}$; and plagioclase from two tonalites (FA-11-12 and FA-10-05) is $An_{74–83}$ and $An_{73–79}$, respectively. Only minor zoning is observed within single grains. For example, An_{76} (core) to An_{83} (rim) from FA-11-12 is the most variation observed in one grain. For comparison, Otamendi *et al.* (2010a)

Table 2: Continued

Sample: Lithology: Canyon:	FA908 grano- diorite Usno	FA11-13A alkali granite leucogr Coral Grande	FA-12–05 metapelite leucogr Cerro Blanco	FA922 metapelite metaseds	FA915 metapelite Usno	FA11-11 metapelite Coral Grande
SiO_2	71·77	78·94	74·85	63·66	56·78	74·70
TiO_2	0·42	0·032	0·834	1·3	1·13	0·346
Al_2O_3	14·07	11·98	11·04	16·37	19·32	13·58
FeO_t	3·17	0·28	3·80	7·77	11·96	2·04
MgO	0·95	0·03	1·50	3·69	4·43	0·62
CaO	3·34	1·30	0·73	3·4	1·06	2·61
Na_2O	2·72	1·84	1·52	2·15	1·02	2·69
K_2O	3·37	5·58	5·58	1·55	4	3·30
Total*	99·70	97·99	98·18	98·23	98·61	98·48
X_{Mg}	0·35	0·14	0·41	0·46	0·40	0·35
Ni	4·4	2	20	57·8	248·4	10
Cr	7·4	5	53	92·8	153·7	4
Sc	14·1	1	9·2	11·7	17·6	6
V	60·8	5	75	159·8	169·1	40
Ba	482	870	351	787	762	489
Rb	65·4	73·8	104·8	47·0	61·7	69·9
Sr	128	93	176	180	147	191
Zr	123	11	508	422	210	144
Y	7·64	0·46	36·73	7·45	7·69	21·03
La	14·25	6·64	55·96	29·35	27·35	42·36
Ce	24·98	9·59	113·88	53·43	46·25	86·31
Pr	2·83	0·91	13·18	5·66	4·67	9·78
Nd	10·96	2·92	48·82	19·71	16·39	35·97
Sm	2·12	0·39	9·55	3·22	2·66	7·06
Eu	1·04	0·86	1·96	1·73	2·48	2·03
Gd	1·89	0·22	7·97	2·28	2·01	5·91
Tb	0·27	0·02	1·24	0·28	0·28	0·86
Dy	1·52	0·10	7·26	1·48	1·53	4·61
Ho	0·31	0·02	1·44	0·30	0·32	0·83
Er	0·82	0·04	3·88	0·84	0·95	2·04
Tm	0·12	0·01	0·57	0·13	0·15	0·26
Yb	0·76	0·04	3·64	0·98	1·05	1·49
Lu	0·13	0·01	0·57	0·20	0·19	0·24
U	0·25	0·10	3·05	0·47	0·37	0·54
Th	0·33	0·93	19·15	2·55	4·52	13·92
Hf	3·23	0·42	13·45	11·41	5·92	3·86

(continued)

reported SVF plagioclase compositions from an ultramafic cumulate body ranging from An_{94} to An_{99}; plagioclase from a hornblende gabbronorite yielded compositions ranging from An_{89} to An_{92}.

DISCUSSION

Mafic zone parent magma

High-X_{Mg} rocks exposed within the mafic zone constrain the composition of the parental magma to the Valle Fértil mafic complex. The rocks with the highest X_{Mg} are olivine websterites and relict troctolites and occur as lenses or bodies meters to hundreds of meters thick. Olivines from the ultramafic cumulates (X_{Mg} = 0·77–0·82; Otamendi *et al.*, 2010*a*) are in equilibrium with a crystallizing melt with X_{Mg} of 0·54–0·62 [assuming a $K_D^{(ol–liq)}$(Fe–Mg) = 0·32 (Roeder & Emslie, 1970)]. These calculated melt X_{Mg} values are too low to be in equilibrium with the mantle, suggesting that the parental magmas experienced some differentiation prior to crystallizing the ultramafic cumulates. Basal dunites and pyroxenites observed in the Kohistan and

Talkeetna complexes (DeBari & Mortensen, 1994; Jagoutz *et al.*, 2006) are perhaps analogs for cumulates crystallized from parental magmas prior to ascent to the level exposed at the SVF.

Otamendi *et al.* (2010*a*), in their study of a Valle Fértil ultramafic cumulate body, demonstrated that pyroxene crystallization temperatures were ∼1200°C, with olivine having crystallized at even higher temperatures. Notably, the lithologies of the ultramafic cumulates are indicative of an H_2O-undersaturated crystallizing magma. Amphibole is present interstitially or as overgrowths or reaction rims on pyroxenes, indicating that the water content of the magma was not sufficient to crystallize amphibole at an early stage. Based on this, Otamendi *et al* (2010*a*) inferred an initial water content of ∼1–2%.

Magma evolution recorded in the mafic zone gabbronorite cumulates

With respect to major and trace elements, the mafic to ultramafic rocks exhibit subtle trends. The low-SiO_2 compositions of the gabbronorites are not

Table 2: Continued

| Sample: Lithology: Canyon:	FA917 amp–olv–norite Usno	FA-12-07 websterite Turbante	FA-12-08 troctolite Turbante	FA-12-13 websterite Algarrobo	FA2-11-01B relict troctolite Usno	FA2-11-13 relict troctolite Coral Grande
SiO_2	45·28	43·05	42·00	46·98	45·60	46·03
TiO_2		0·181	0·076	0·446	0·144	0·159
Al_2O_3	11·19	5·47	12·13	8·94	25·15	23·09
FeO_t	11·99	14·70	12·16	12·38	4·69	5·19
MgO	21·27	32·60	26·05	21·64	7·02	8·07
CaO	9·04	3·21	7·02	8·13	16·51	16·69
Na_2O	0·48	0·38	0·34	0·90	0·62	0·59
K_2O	0·32	0·14	0·02	0·32	0·18	0·08
Total*	98·06	93·64	94·41	99·02	98·71	97·44
X_{Mg}	0·76	0·80	0·79	0·76	0·73	0·73
Ni	453·8	742	440	527	85	84
Cr	926·1	1175	368	2292	445	545
Sc	28·5	16·4	11·4	33·6	25·4	29·4
V	112·9	85	50	175	80	96
Ba	52	32	9	140	81	24
Rb	10·6	3·3	0·5	10·7	4·0	1·9
Sr	90	47	90	103	218	208
Zr	17	14	3	31	6	6
Y	5·89	4·57	1·20	9·57	3·02	3·30
La	2·64	2·35	0·43	5·97	1·03	1·22
Ce	6·79	5·47	0·95	11·51	2·38	2·80
Pr	0·94	0·76	0·13	1·45	0·32	0·39
Nd	4·24	3·37	0·58	6·29	1·56	1·80
Sm	1·11	0·88	0·18	1·60	0·47	0·55
Eu	0·29	0·21	0·09	0·49	0·24	0·22
Gd	1·13	0·88	0·20	1·81	0·53	0·62
Tb	0·19	0·15	0·03	0·31	0·09	0·11
Dy	1·18	0·91	0·22	1·88	0·60	0·65
Ho	0·24	0·18	0·05	0·39	0·13	0·14
Er	0·64	0·51	0·13	1·08	0·34	0·36
Tm	0·09	0·08	0·02	0·15	0·05	0·05
Yb	0·57	0·47	0·14	0·96	0·30	0·32
Lu	0·08	0·07	0·02	0·14	0·05	0·05
U	0·22	0·13	0·02	0·49	0·04	0·07
Th	0·86	0·57	0·09	2·26	0·14	0·22
Hf	0·61	0·44	0·09	0·84	0·20	0·21

*Pre-normalization totals.
gn, gabbronorite.

representative of melts and they appear to be the cumulate product of a liquid line of descent (*sensu lato*). This evolution is illustrated by the Z-shaped pattern observed in the X_{Mg} vs SiO_2 plot (see Fig. 6). Whole-rock X_{Mg} values of the mafic rocks decrease from 0·8 to ~0·65 with increasing SiO_2, at which point the trend turns and SiO_2 decreases with decreasing X_{Mg}. A similar inflection is also observed in the SiO_2 vs TiO_2 trend. This and other compositional (FeO, V) and modal data suggest the inflection of the SiO_2 vs X_{Mg} (and TiO_2) trend corresponds to the onset of Fe–Ti oxide crystallization and accumulation. At X_{Mg} of ~0·4 and 42% SiO_2, there is another inflection in the trend. The samples that fall near this second inflection are marked by the greatest abundances of Fe–Ti oxides (~5–8 vol. %), and, correspondingly, the highest FeO (~20 wt %) and TiO_2 (~1·8 wt %) concentrations. From this point the compositions range to higher SiO_2 values with slightly decreasing X_{Mg}—a typical trend for intermediate arc rocks. Jagoutz *et al.* (2011) reported a similar Z-shaped X_{Mg} vs SiO_2 trend for the Southern Plutonic Complex of the Kohistan batholith. There, the compositional spectrum begins at higher X_{Mg} (~0·9) and some rock types are garnetiferous (Jagoutz *et al.*, 2007, 2011).

Clinopyroxene compositions yield additional evidence for the evolution of the crystallizing magma. As with olivine, the X_{Mg} of clinopyroxene can be used to estimate the X_{Mg} of the melt with which it is in equilibrium [assuming a $K_D^{(cpx–liq)}$(Fe–Mg) = 0·27; Sisson & Grove, 1993; Pichavant & Macdonald, 2007]. For the SVF rocks, clinopyroxene X_{Mg} (and calculated melt X_{Mg}) decreases with whole-rock X_{Mg}, but the whole-rock and calculated melt X_{Mg} do not have a 1:1 correlation (Fig. 11). Instead, rocks with high X_{Mg} (>0·45) fall above the 1:1 line—with whole-rock X_{Mg} being greater than calculated melt X_{Mg}—suggesting that they accumulated Mg-rich phases (such as olivine and orthopyroxene) in the melt from which they crystallized. Notably, several samples with <45 wt % SiO_2 have calculated melt X_{Mg} < 0·45 (and whole-rock X_{Mg} of <0·45), indicating that they probably crystallized from a more evolved magma.

The geochemical trends and the clinopyroxene compositions indicate that the gabbronorite suite is a
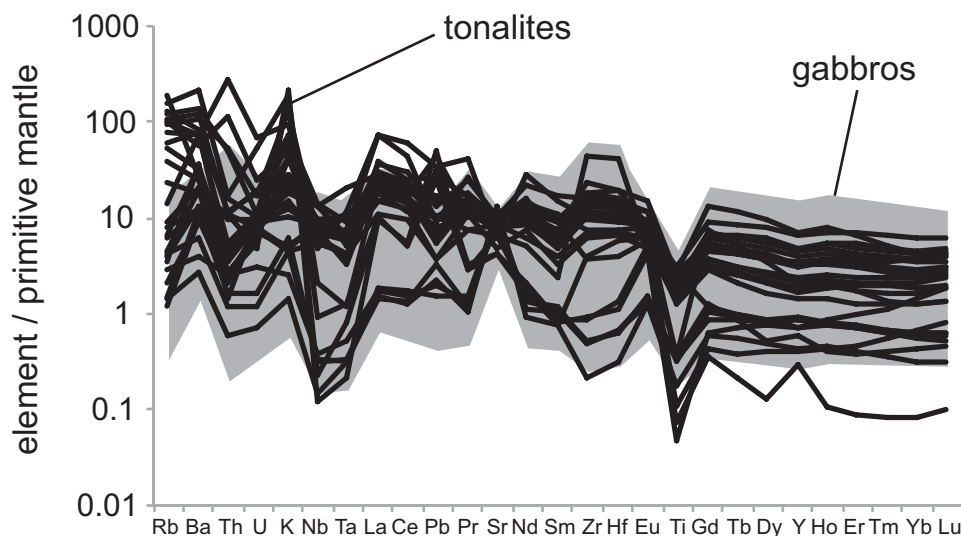
Fig. 7. Primitive mantle-normalized trace element patterns for the SVF tonalites. Primitive mantle values from Sun & McDonough (1989). The gray field represents the range of compositions of SVF gabbros (<51% SiO_2). There is overall similarity between the patterns for the tonalites and the more mafic rocks, although some tonalites are more enriched in elements that are incompatible with a gabbroic mineral assemblage (Rb, Ba, K, LREE).

cumulate or residual assemblage. We rarely observe cumulus textures such as monomineralic banding or size sorting. However, primary igneous features such as inclusions, small pegmatites, veinlets, and local modal layering are preserved; consequently, subsequent metamorphic re-equilibration was limited, probably to the grain scale. It is also likely that repeated disruption and mixing of the crystal mush by open-system processes disrupted the gradual accumulation of crystals from a stagnant or weakly convecting melt.

Tonalites in the mafic zone

Tonalites form a significant portion (~40% by area) of the SVF mafic zone. There are many subtle differences between the tonalites of the SVF mafic zone and those higher in the section in the intermediate and silicic zones. The most significant difference is that the mafic zone tonalites have a low K_2O concentration (<1 wt %, with many less than 0·5 wt %; see Fig. 6) with respect to the silicic zone tonalites (~2 wt % K_2O). In general, the tonalites from the mafic zone are also less silicic than those higher in the section. Additionally, at any given silica content, mafic zone tonalites tend to have slightly higher concentrations of MgO and CaO, and lower concentrations of Rb, Ba, and light REE (LREE) (see Figs 6 and 8).

Tonalites in the SVF mafic zone are heterogeneous, complexly interlayered and gradational into the gabbro-norites. Tonalitic material is also present as stringers, patches, and veins in many of the gabbronoritic rocks (see Fig. 3). One sample of such a leucotonalite vein (FA-12-14) is indistinguishable from the more massive, low-K tonalitic domains. We were unable to identify many field relations that unambiguously demonstrate the process by which the magma differentiated—only that tonalite coexists with gabbronorite in outcrop and

that ostensibly the two were segregated, or in the process of being segregated, from one another (Zavala et al., 2011; Putirka et al., 2014). Below, we explore a petrogenetic model in which we relate the gabbronor-ites and the tonalites through fractional crystallization.

Petrogenetic model

Comprehensive petrogenetic models for the Sierra Valle Fértil suite (mafic to felsic rocks) have been previously presented, although these models do not adequately describe the compositional variation of all the SVF rocks (Otamendi et al., 2009a, 2010a, 2012). Because the compositions of the low-K tonalites of the SVF mafic zone are distinct from those found elsewhere in the suite, we treat these data separately. Here we provide a fractional crystallization model for major and trace elements to explore the genetic relationship of mafic zone gabbronorites and tonalites. From a starting composition cumulate compositions are removed in steps. The cumulate composition is changed with each fractionation step. This model is explicitly linked to the geology of the SVF: the cumulate composition removed at any given step is a calculated average composition of a mafic to ultramafic subgroup from the SVF mafic complex. Essentially, observed whole-rock compositions are used for cumulates, rather than inferred crystallizing assemblages and fixed distribution coefficients (see Jagoutz, 2010; Bucholz et al., 2014).

The starting composition for the SVF model (see Table 9) was calculated by averaging three SVF mafic rocks with X_{Mg} from 0·55 to 0·6. One of these (FA-11-01) is a mafic dike; the other two (FA-12-17 and FA-09-18) are mafic rocks with relatively non-cumulate compositions (~50–52% SiO_2, Eu/Eu* = 0·7–0·75). This starting composition is consistent with olivine and clinopyroxene compositions that suggest that the parental magma
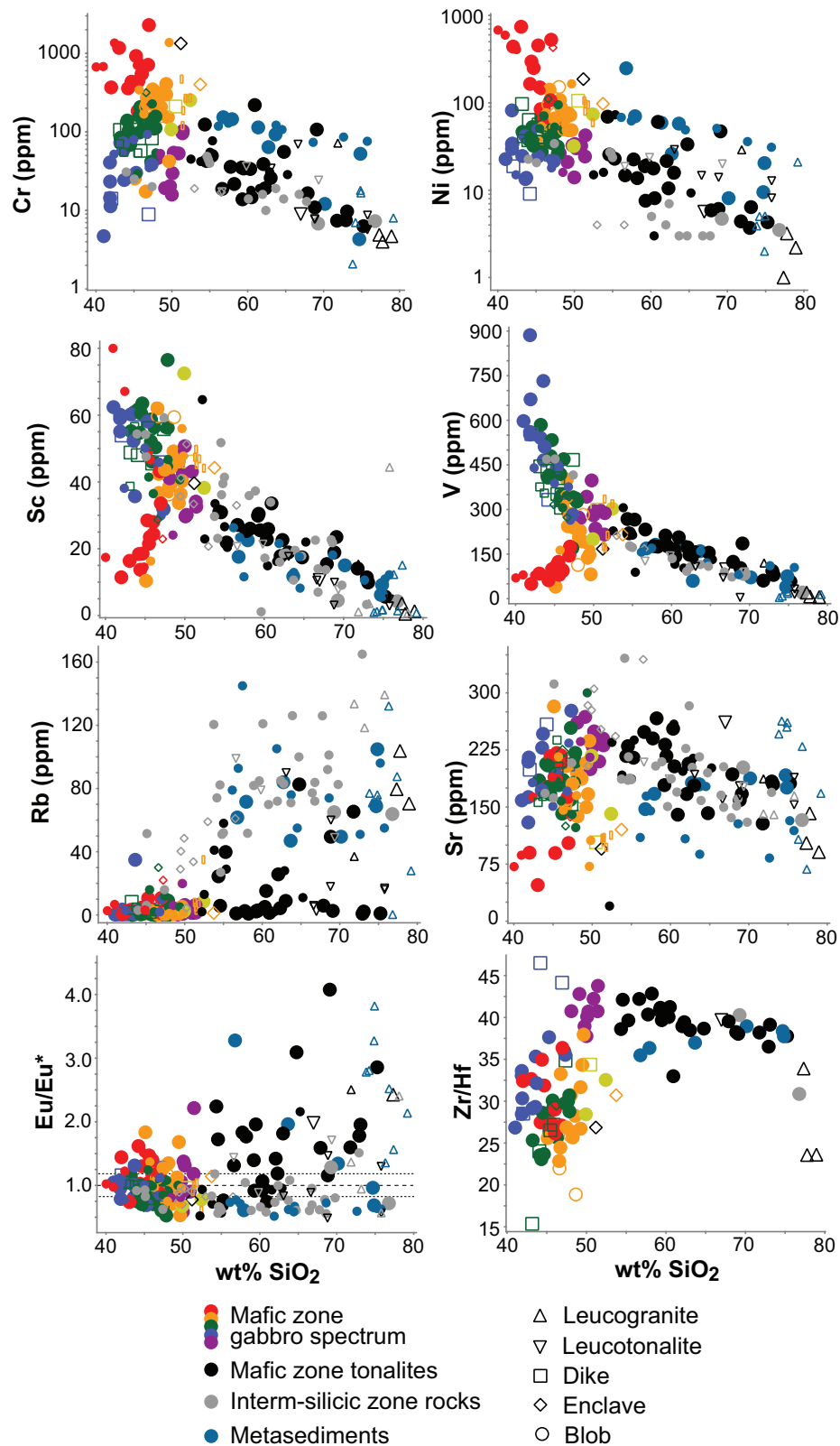
Fig. 8. Trace element variations vs SiO$_2$ for the SVF. The gabbroic rocks of the mafic zone rocks are color-coded as in Fig. 6. Tonalites of the mafic zone are shown in black. Rocks from the intermediate and silicic zones are colored gray; metasedimentary rocks are colored blue. Other types of sample (dike, enclave, blob, leucogranite, leucotonalite) are identified by separate symbols. Large symbols are data from this study, and smaller symbols are samples from previous studies (Otamendi *et al.*, 2008, 2009*b*, 2010*a*, 2010*b*, 2012).
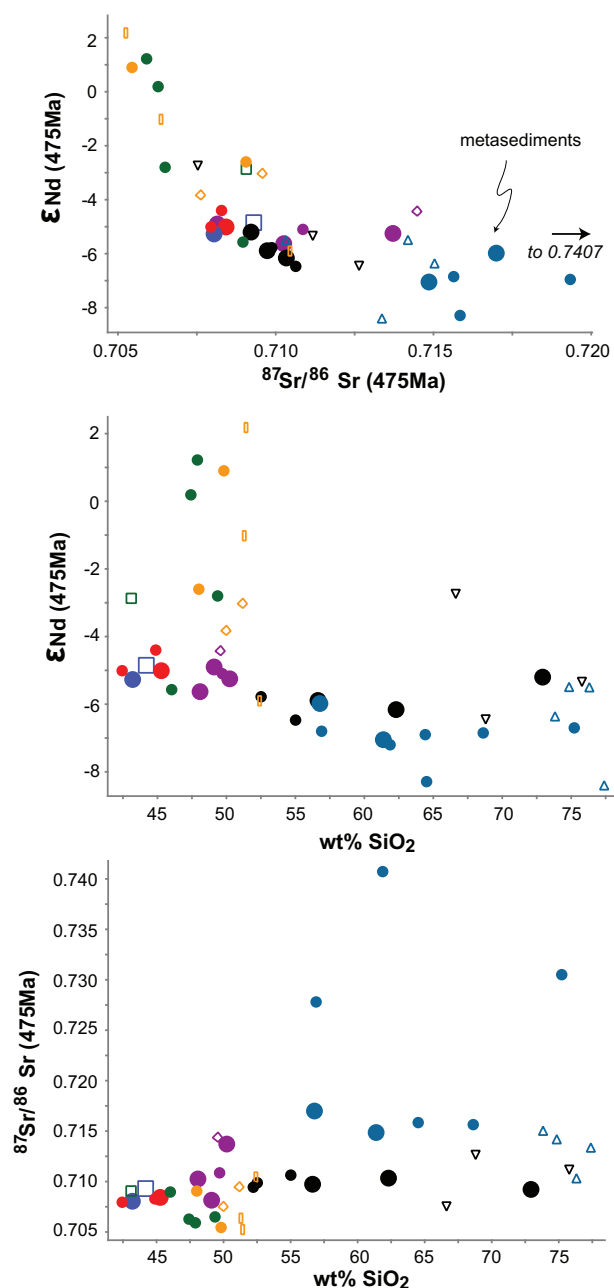
Fig. 9. Isotopic compositions (^{87}Sr/^{86}Sr and ε_{Nd}, both age-corrected to 475 Ma) of the SVF mafic zone rocks and associated metasediments. Data for each isotopic system are also plotted vs SiO$_2$. It should be noted that even the most silica-deficient rocks are significantly contaminated (high ^{87}Sr/^{86}Sr, low ε_{Nd}) with respect to primitive mantle. For the magmatic rocks there is no significant correlation of either isotopic system with SiO$_2$. Symbols as in Fig. 8.

to the exposed SVF magma system was not a mantle-equilibrated primitive basaltic melt. The concentrations of several trace elements (notably Sr, Y, Sc, and REE) were adjusted from the calculated starting composition to provide a better fit for the model, although these adjustments were always within the range of concentrations for the three rocks used for the starting composition average.

From the starting composition, five distinct cumulate compositions were progressively subtracted over five steps to derive residual liquids (the 'liquid line of descent'; Fig. 12). The mass-balance equation used to calculate the concentration for any given element—major or trace—at each step is

$$D = (M - XC)/(1 - X)$$

where D is the elemental concentration in the daughter magma, M is the elemental concentration in the starting magma, C is the elemental concentration of the cumulate removed during that step, and X is the fraction of cumulate removed during the step (e.g. $X = 0.2$ for 20% removal). Each of the five cumulate compositions used in the model is an average of one of the compositional groups identified on the X_{Mg} vs SiO$_2$ trend (Fig. 13; Table 9). The model proceeds by first subtracting out a chosen percentage of cumulate group 1. From the daughter magma derived from that first step, a percentage of cumulate group 2 is subtracted. From that daughter magma, a percentage cumulate group 3 is subtracted, and so on.

From the starting composition the best-fit model subtracts, stepwise, 20% of cumulate group 1, 15% of group 2, 10% of group 3, 30% of group 4, and 30% of group 5, for a maximum of 70% crystals removed relative to the original magma ($F = 0.3$). The most evolved daughter magma produced in this model is a tonalite with 62% SiO$_2$. This fractionation model is consistent with the production of the <62% SiO$_2$ tonalites observed in the field. One important distinction of this model is that this fractionation pathway is forced to produce the same 'cumulate line of descent', consistent with compositional data from the SVF cumulates (ultramafic cumulates and hornblende gabbronorites). For the model to fit, the crystallization sequence must proceed in its correct order, regardless of where it is stopped (for example, first removing 20% of cumulate group 1, then 15% of cumulate group 2, then 10% of cumulate group 3, etc.).

Discussion of the petrogenetic model

Much of the SVF mafic zone compositional array below 62 wt % SiO$_2$ is consistent with an origin by fractional crystallization in which the mafic rocks are the cumulate assemblages and the silicic rocks are the daughter magmas. However, it is difficult to field-test the cumulate volumes that our model implies. With the exception of the olivine-bearing samples, the cumulate rocks from the different groups are all gabbronorites and appear very similar in hand sample, making it extremely difficult to distinguish between the gabbronorite varieties in the field. For this model, the cumulate volumes—per cent fractionated—were chosen so as to generate the best fit for the residual liquid to the tonalites within the mafic zone. We do not, then, place special importance on these exact volumes of cumulates, although they do provide the best fit.

Table 3: Radiogenic isotopic compositions of Sierra Valle Fértil rocks

Sample: Lithology:	FA0907 qtz-gabbro enclave	FA0909 hbl gabbro	FA0911 tonalite	FA0912 tonalite	FA0914 qtz-gabbro	FA0915 metapelite	FA0917 hbl-olv websterite	FA0920 gabbro	FA1012 hbl gabbronorite	FA1013 metapelite	FA1014 tonalite	FA1018 leucogranite
Rb (ppm)	0.146	1.684	0.863	0.832	4.531	64.429	9.220	2.708	0.302	65.614	2.917	120.364
Sr (ppm)	268.843	267.233	261.488	190.865	271.378	170.686	87.134	271.419	194.771	161.088	209.712	91.769
Rb/Sr	0.0005	0.0063	0.0033	0.0044	0.0167	0.3775	0.1058	0.0100	0.0015	0.4073	0.0139	1.3116
$^{87}Rb/^{86}Sr$	0.001565	0.018128	0.009492	0.012534	0.048041	1.087206	0.304351	0.028702	0.004452	1.172990	0.040018	3.784979
$^{87}Sr/^{86}Sr(0)$	0.708159	0.709425	0.709795	0.709303	0.714039	0.724324	0.710480	0.710450	0.708076	0.722769	0.710607	0.744117
$^{87}Sr/^{86}Sr$ SE%	0.0012	0.0029	0.0015	0.001	0.0017	0.0011	0.0017	0.0009	0.0012	0.0008	0.0016	0.0026
$^{87}Sr/^{86}Sr(475$ Ma$)$	0.708148	0.709303	0.709731	0.709218	0.713715	0.716991	0.708427	0.710256	0.708046	0.714857	0.710337	0.718587
Sm (ppm)	7.911	10.181	3.08	1.707	3.373	2.186	1.089	7.729	1.519	1.726	3.321	0.175
Nd (ppm)	33.181	39.727	13.524	8.219	17.842	15.91	4.1998	30.048	5.338	11.566	15.53	2.3876
Sm/Nd	0.2384	0.2563	0.2277	0.2077	0.1890	0.1374	0.2593	0.2572	0.2982	0.1492	0.2138	0.0733
$^{147}Sm/^{144}Nd$	0.144136	0.154925	0.137675	0.125572	0.114268	0.083043	0.156875	0.155490	0.180295	0.090200	0.129249	0.044344
$^{143}Nd/^{144}Nd(0)$	0.512223	0.512259	0.512152	0.512150	0.512112	0.511978	0.512257	0.512221	0.512316	0.511945	0.512112	0.511850
$\varepsilon_{Nd}(0)$	-8.1	-7.4	-9.5	-9.5	-10.3	-12.9	-7.4	-8.1	-6.3	-13.5	-10.3	-15.4
$^{143}Nd/^{144}Nd(475$ Ma$)$	0.511775	0.511778	0.511724	0.511760	0.511757	0.511720	0.511770	0.511738	0.511756	0.511665	0.511710	0.511712
$\varepsilon_{Nd}(475$ Ma$)$	-4.9	-4.8	-5.9	-5.2	-5.3	-6.0	-5.0	-5.6	-5.3	-7.1	-6.2	-6.1
$^{143}Nd/^{144}Nd$ SE%	0.0016	0.0012	0.0011	0.0018	0.0021	0.0022	0.0025	0.0013	0.0019	0.0012	0.0015	0.0021
$^{206}Pb/^{204}Pb$	18.4453	18.4943	18.4218	18.7126	18.4799	18.2749	18.7270	18.3722	18.5492	18.3642	18.3254	16.9395
$^{207}Pb/^{204}Pb$	15.6606	15.6585	15.6537	15.6490	15.7984	15.6502	15.6606	15.6588	15.6528	15.6564	15.6510	15.4941
$^{208}Pb/^{204}Pb$	38.2196	38.4126	38.1935	38.2066	38.4923	38.3435	38.5526	38.1780	38.2973	38.4878	38.1487	36.7177

*Pb standard error (SE): $^{206}Pb/^{204}Pb$ = 0.0034; $^{207}Pb/^{204}Pb$ = 0.0035; $^{208}Pb/^{204}Pb$ = 0.0089; Pb data age corrected to 475 Ma.
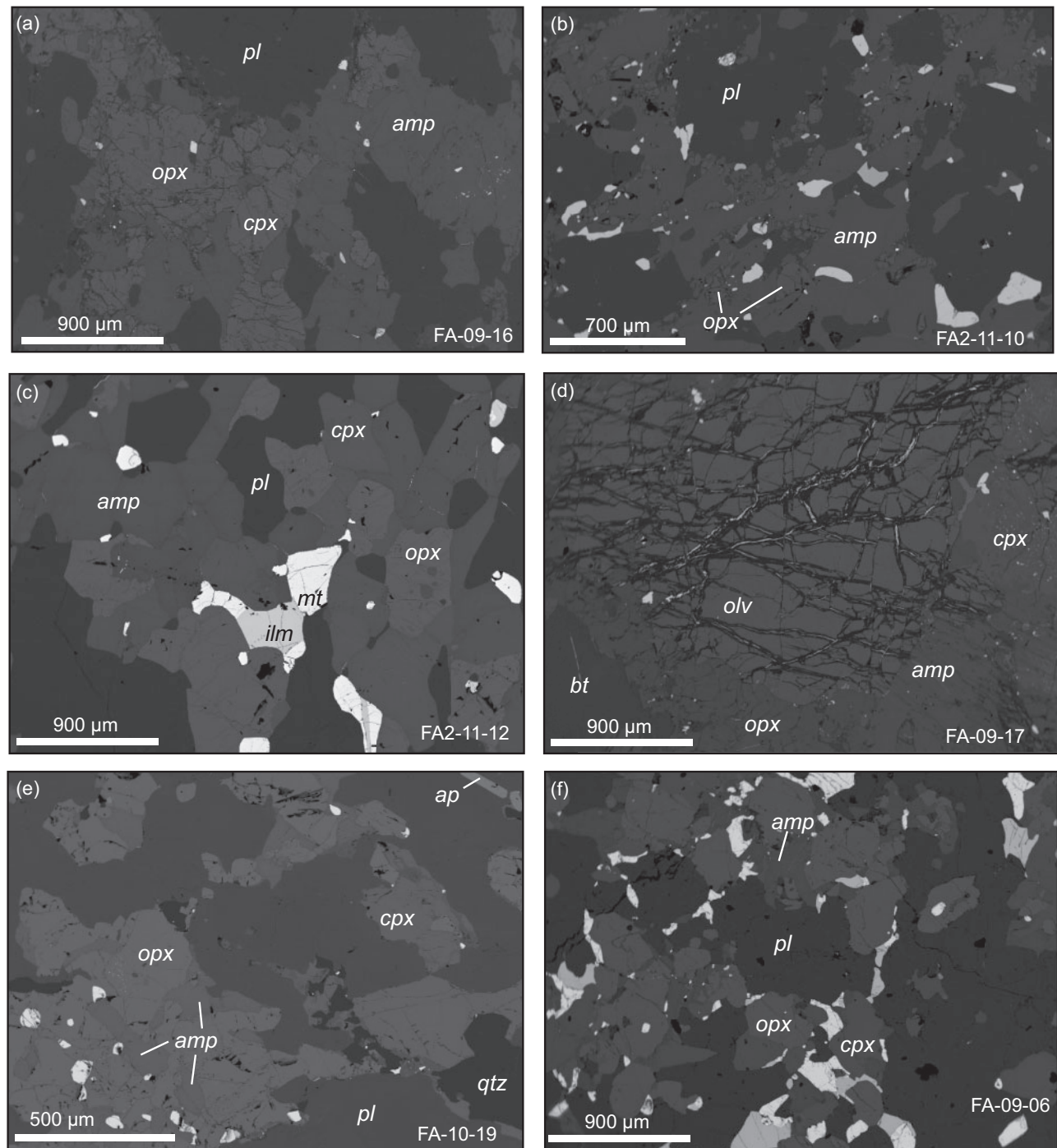
Fig. 10. Back-scattered electron images for the SVF mafic zone rocks, including gabbronorite (a, c, f), gabbro dike (b), amphibole–olivine gabbronorite (d), and tonalite (e). The lack of euhedral grains [with the exception of apatite in (e)] and the total lack of zoning in any mineral should be noted. A consertal texture is common (a, b, e, f), as is a granoblastic texture (c). It should be noted in (d) that the olivine is heavily altered to serpentine, but that fresh domains persist.

There is a significant degree of scatter in the tonalite compositions. This is probably due to additional processes not considered in our simple fractionation model, such as magma mixing and small degrees of assimilation (see Jagoutz, 2010; Putirka *et al.*, 2014). We do not take into account isotopes in our fractionation model (see Otamendi *et al.*, 2012). Additionally, we have not attempted to model the generation of tonalites with >62% SiO_2. Above 62% SiO_2, a more complex set of assimilation, mixing, and fractionation processes control compositional diversity. For example, Na_2O decreases with increasing SiO_2 beginning at ~62% SiO_2, probably the result of the saturation of an increasingly sodic plagioclase with progressive fractionation, an effect not

Table 4: Major element compositions of selected olivine from SVF rocks

	FA-12-07	FA-12-07	FA-12-07	FA-12-07	FA-12-08	FA-12-08	FA-12-08	FA-12-08
SiO_2	40·02	39·49	39·18	39·27	39·46	38·95	38·5	39·16
Cr_2O_3	0·00	0·00	0·00	0·01	0·01	0·00	0·00	0·00
FeO	17·69	18·36	18·26	18·16	19·38	19·50	18·85	19·33
MnO	0·27	0·35	0·21	0·27	0·28	0·27	0·24	0·22
MgO	41·83	41·65	42·25	42·20	40·75	41·17	42·32	41·18
CaO	0·01	0·00	0·00	0·00	0·01	0·01	0·02	0·01
NiO	0·16	0·15	0·10	0·09	0·11	0·11	0·07	0·10
Pre-norm total	99·18	99·12	99·40	99·54	99·75	99·61	100·20	99·70
Fo %	80·57	79·88	80·30	80·32	78·70	78·78	79·77	78·96
X_{Mg} olivine	0·81	0·80	0·80	0·80	0·79	0·79	0·80	0·79
X_{Mg} of melt*	0·55	0·54	0·55	0·55	0·53	0·53	0·54	0·53
T(liquidus)†	1249	1245	1248	1248	1240	1240	1245	1241

	FA-12-13	FA-12-13	FA-12-13	FA-12-13	FA-09-17	FA-09-17	FA-09-17	FA-09-17
SiO_2	39·34	39·41	39·18	39·23	38·95	38·47	38·48	38·37
Cr_2O_3	0·00	0·01	0·00	0·00	0·00	0·00	0·02	0·00
FeO	17·04	16·74	17·30	17·30	20·65	21·24	20·47	21·41
MnO	0·26	0·30	0·28	0·28	0·28	0·29	0·28	0·28
MgO	43·16	43·29	43·02	42·95	39·98	39·87	40·58	39·80
CaO	0·01	0·00	0·01	0·00	0·03	0·01	0·01	0·00
NiO	0·20	0·25	0·21	0·22	0·12	0·13	0·15	0·13
Pre-norm total	99·11	99·75	100·27	100·31	99·12	99·54	99·32	99·42
Fo %	81·63	81·90	81·34	81·31	77·27	76·73	77·70	76·58
X_{Mg} olivine	0·82	0·82	0·81	0·81	0·77	0·77	0·78	0·77
X_{Mg} of melt*	0·57	0·58	0·57	0·57	0·50	0·50	0·51	0·50
T(liquidus)†	1254	1256	1253	1253	1233	1231	1235	1230

*X_{Mg} melt assumes a $K_D^{(ol–liq)}$(Fe–Mg) = 0·32 (Roeder & Emslie, 1970; Pichavant & Macdonald, 2007).
†Liquidus T from Niu *et al.* (2002).

taken into account by our model. K_2O remains low (<1 wt %) in most mafic zone tonalites, even those with >73% SiO_2; hence it is likely that these high-SiO_2, low-K, low-Na tonalites do not represent liquid compositions but have lost melt or fluid rich in K and Na.

Numerous experiments demonstrate that a range of tonalite compositions can be readily generated via partial melting of a basaltic or amphibolitic source (Beard & Lofgren, 1989; Rapp, 1991; Wolf & Wyllie, 1994; Beard, 1995; Rapp & Watson, 1995; Sisson *et al.*, 2005; Saito *et al.*, 2007). Although the compositions of the SVF mafic zone tonalites are exceptionally low-K and low-Na, they are not altogether dissimilar from tonalites produced experimentally by partial melting. Arc rocks similar in composition to the SVF mafic zone tonalites have been reported elsewhere and interpreted to be the result of partial melting (Beard, 1997; Kawate & Arima, 1998; Haraguchi *et al.*, 2003; Saito *et al.*, 2004; Smith *et al.*, 2006). However, in the SVF mafic zone we see very little direct evidence supporting a partial melting relationship between the mafic and silicic rocks. We interpret the gabbronorites to be the result of phenocryst accumulation; their modes and compositions display distinctive trends that are not consistent with the residues of partial melting experiments [see fig. 3 of Jagoutz *et al.*, (2011)]. Furthermore, manifest field relations indicating interspersed and intermingled bodies of gabbronorite and tonalite are more consistent with a complex series of intrusive and local melt extraction events. We do not find geological or petrographic evidence that partial melting, as expressed by amphibole breakdown, is a dominant process generating the silicic rocks.

SiO_2 enrichment: the importance of amphibole and Fe–Ti oxides

The process of silica enrichment in a fractionating basaltic magma is problematic because plagioclase and pyroxene—the two most common crystallizing minerals in basalts—have essentially the same composition as the magma. A liquid separated from a plagioclase–pyroxene cumulate would be very similar with respect to its silica content—the so-called 'gabbro barrier' (Davidson *et al.*, 2007; Jagoutz, 2010). For silica enrichment to occur, low-SiO_2 phases such as olivine, garnet, amphibole, and Fe–Ti oxides must be retained in the cumulate relative to the expelled liquid (Bergantz, 1991; Claeson & Meurer, 2004; Davidson *et al.*, 2007; Dessimoz *et al.*, 2012; Smith, 2014). Garnet is excluded in our discussion because we find no igneous garnet in the SVF mafic rocks. Olivine is observed only in the ultramafic cumulates. Amphibole and Fe–Ti oxides, however, are abundant in the SVF rocks.

Amphibole is ubiquitous in the Valle Fértil crustal section and forms anywhere from ~5 to ~40% of the gabbronorites, although it is rarely found as discrete, sub- to euhedral grains. It is typically present as rims on pyroxenes, and as oikocrysts ranging from ~1 to 5 cm in diameter. It is also observed as the dominant mafic

Table 5: Major element compositions of selected clinopyroxene from SVF rocks

| Sample: | FA2-11-12 | FA2-11-12 | FA2-11-12 | FA2-11-12 | FA-10-19 | FA-10-19 | FA-10-19 | FA-10-19 |
Lithology:	hbl gn	hbl gn	hbl gn	hbl gn	tonalite	tonalite	tonalite	tonalite
SiO_2	51·18	51·20	51·24	52·16	52·10	52·06	52·77	52·39
TiO_2	0·41	0·40	0·42	0·27	0·25	0·32	0·13	0·22
Al_2O_3	3·04	2·99	3·19	2·31	2·48	2·42	1·48	2·25
Cr_2O_3	0·00	0·01	0·00	0·00	0·08	0·08	0·05	0·08
FeO	8·54	8·21	9·53	7·64	8·92	8·39	6·89	8·00
MnO	0·32	0·34	0·37	0·30	0·28	0·29	0·27	0·30
MgO	13·64	13·62	13·98	14·12	13·89	13·52	14·74	13·98
CaO	22·51	22·87	20·93	22·90	21·62	22·44	23·34	22·38
Na_2O	0·37	0·36	0·34	0·30	0·38	0·49	0·32	0·40
Total	100·87	100·01	99·36	99·78	99·31	99·37	99·57	100·06
X_{Mg} cpx	0·79	0·79	0·81	0·79	0·78	0·76	0·81	0·78
X_{Mg} melt*	0·43	0·44	0·41	0·47	0·43	0·44	0·51	0·46
Wo	46·74	47·42	43·77	47·20	45·13	46·94	47·41	46·55
En	39·42	39·30	40·68	40·50	40·34	39·36	41·67	40·46
Fs	13·84	13·29	15·55	12·29	14·53	13·70	10·92	12·99

| Sample: | FA2-11-02 | FA2-11-02 | FA-11-02 | FA-11-02 | FA-09-16 | FA-09-16 | FA-09-17 | FA-09-17 |
Lithology:	hbl gn	hbl gn	hbl gn	hbl gn	hbl gn	hbl gn	amph–olv norite	amph–olv norite
SiO_2	51·91	51·23	51·75	52·28	52·62	51·82	51·80	51·39
TiO_2	0·07	0·11	0·10	0·04	0·04	0·12	0·22	0·17
Al_2O_3	2·38	2·70	2·25	2·36	1·99	2·54	3·31	4·20
Cr_2O_3	0·00	0·00	0·00	0·00	0·00	0·00	0·14	0·11
FeO	9·41	10·82	9·96	8·80	7·76	8·22	4·78	5·59
MnO	0·38	0·43	0·40	0·33	0·20	0·20	0·12	0·20
MgO	13·31	13·60	13·29	13·55	14·20	14·03	15·61	14·98
CaO	22·06	20·60	21·76	22·18	22·81	22·63	23·79	23·07
Na_2O	0·48	0·51	0·49	0·46	0·38	0·46	0·23	0·29
Total	99·79	99·17	100·12	99·70	100·41	100·01	99·56	99·36
X_{Mg} cpx	0·76	0·79	0·76	0·76	0·79	0·80	0·89	0·87
X_{Mg} melt*	0·41	0·38	0·39	0·43	0·47	0·45	0·61	0·56
Wo	46·03	42·94	45·31	46·30	46·91	46·60	48·31	47·79
En	38·64	39·45	38·50	39·36	40·63	40·19	44·11	43·18
Fs	15·33	17·61	16·19	14·34	12·46	13·21	7·58	9·04

*X_{Mg} (melt) assumes a $K_D^{(cpx-liq)} = 0.27$ (Sisson & Grove, 1993; Pichavant & McDonald, 2007).

mineral in gabbroic dikes and in a few relict troctolites. Texturally, then, it appears that amphibole either replaces other minerals or was a late phase on the liquidus of the Valle Fértil magmas. Nevertheless, other compositional trends, such as depleted Zr/Hf in amphibole gabbronorites and steepening REE trends with increasing SiO_2 [although Dy/Yb does not change appreciably (see Davidson *et al.*, 2007)] indicate that amphibole crystallization exerted an influence on the fractionating magma compositions, like that commonly reported in xenoliths from arcs (Smith, 2014).

In addition to amphibole, Fe–Ti oxide fractionation produces silica enrichment. In the SVF, magnetite and ilmenite appear in all gabbronorites. The cumulate subgroups, as identified on the X_{Mg} vs SiO_2 plot, have notable differences in Fe–Ti oxide abundances. Fe–Ti oxides increase in abundance with progression along the 'cumulate line of descent'. High-X_{Mg} rocks (> ∼0·6; red and orange cumulate groups in Fig. 13) have trace amounts of Fe–Ti oxides. Intermediate-X_{Mg} rocks (0·5–0·6; green cumulate group) have appreciable Fe–Ti oxides (<∼3% magnetite, <∼1·2% ilmenite). Cumulates with the lowest X_{Mg} (∼0·4–0·5; blue cumulate group) and the lowest SiO_2 (∼41–45%) are particularly rich in

magnetite and ilmenite (∼4% and ∼1–2% respectively, with consequently high concentrations of TiO_2 and FeO; Fig. 14; see also Fig. 6). It is notable that there is no such relationship between amphibole mode and whole-rock composition. Hence it is likely that the accumulation of Fe–Ti oxides is perhaps more important than amphibole in producing silica enrichment in some arc rocks. The extreme abundances of Fe–Ti oxides in certain cumulate lithologies suggest that, in the fractionation sequence, Fe–Ti oxide 'blooms' may occur, perhaps during recharge of mafic magmas or when the thermodynamic or magmatic state favors increased crystallization and accumulation.

Assimilation of country rock

The Famatinian arc was constructed on, and within, a fertile, miogeoclinal sequence on the edge of the proto-South American continent (Otamendi *et al.*, 2008; Cristofolini *et al.*, 2012). It therefore should not be viewed as an 'Andean' arc because it was not emplaced within an old, thick craton (Ducea *et al.*, 2010). Neither should it be viewed as an island arc, because it was constructed on the edge of a continent. Petrogenetic

Table 6: Major element compositions of selected orthopyroxene from SVF rocks

| Sample: | FA2-11-12 | FA2-11-12 | FA2-11-12 | FA2-11-12 | FA-10-19 | FA-10-19 | FA-10-05 | FA-10-05 |
Lithology:	hbl gn	hbl gn	hbl gn	hbl gn	tonalite	tonalite	tonalite	tonalite
SiO_2	52·52	52·56	52·41	52·86	52·91	52·46	51·87	52·14
TiO_2	0·13	0·08	0·08	0·08	0·08	0·09	0·09	0·08
Al_2O_3	1·52	1·37	1·30	1·16	1·14	1·01	1·44	1·36
Cr_2O_3	0·02	0·02	0·01	0·01	0·03	0·03	0·00	0·01
MnO	0·89	0·80	0·77	0·85	0·66	0·86	1·13	1·18
MgO	22·77	22·60	22·79	22·69	22·44	21·48	21·02	21·34
FeO	21·62	22·25	22·19	21·90	22·30	23·64	23·90	23·37
CaO	0·53	0·32	0·45	0·45	0·44	0·42	0·54	0·52
Na_2O	0·01	0·00	0·00	0·00	0·00	0·00	0·00	0·00
Total*	99·62	99·59	99·44	99·28	99·03	99·06	99·57	98·95
X_{Mg}	0·65	0·64	0·65	0·65	0·64	0·62	0·61	0·62
En	64·54	64·00	64·09	64·28	63·64	61·30	60·38	61·28
Fs	34·37	35·34	35·00	34·80	35·47	37·84	38·51	37·64
Wo	1·09	0·66	0·92	0·92	0·89	0·86	1·12	1·07

| Sample: | FA2-11-02 | FA2-11-02 | FA-09-16 | FA-09-16 | FA-09-17 | FA-09-17 | FA-09-20 | FA-09-20 |
Lithology:	hbl gn	hbl gn	hbl gn	hbl gn	amph–olv norite	amph–olv norite	norite	norite
SiO_2	51·83	51·18	52·60	52·86	53·88	53·18	51·76	52·16
TiO_2	0·00	0·00	0·00	0·00	0·02	0·07	0·12	0·09
Al_2O_3	1·54	1·63	1·41	1·37	3·14	3·36	1·26	1·17
Cr_2O_3	0·00	0·00	0·00	0·00	0·09	0·07	0·00	0·00
MnO	0·83	0·90	0·59	0·51	0·31	0·30	1·13	1·06
MgO	21·17	20·44	22·63	22·64	28·48	28·56	20·81	21·03
FeO	24·20	25·44	22·36	22·23	13·74	14·00	23·96	24·03
CaO	0·42	0·39	0·40	0·37	0·32	0·45	0·94	0·46
Na_2O	0·01	0·02	0·01	0·02	0·00	0·00	0·00	0·00
Total*	99·78	99·91	99·80	100·47	99·80	99·86	99·32	99·94
X_{Mg}	0·61	0·59	0·64	0·64	0·79	0·78	0·61	0·61
En	60·41	58·41	63·82	64·00	78·20	77·74	59·58	60·36
Fs	38·74	40·78	35·37	35·25	21·16	21·38	38·48	38·69
Wo	0·86	0·81	0·81	0·74	0·64	0·88	1·94	0·95

*Pre-normalization totals.
gn, gabbronorite.

studies based on isotope data from the Kohistan (Petterson *et al.*, 1993; Dhuime *et al.*, 2009; Jagoutz, 2010) and Talkeetna (Rioux *et al.*, 2007) crustal sections—both paleo island arcs—suggest that assimilation of pre-existing country rocks plays only a minor role in contributing to the mass of arc magmas. Some studies on the Bonanza arc have made similar arguments (Cui & Russell, 1995; Larocque & Canil, 2010), although there are differing opinions (see DeBari *et al.*, 1999). The Kohistan and Talkeetna arcs intrude pre-existing crust that is dominantly oceanic in composition, with isotopic characteristics similar to those of typical mantle. However, in the western domain of the Talkeetna complex, isotopic compositions are more variable and are interpreted to reflect the influence of the adjacent Wrangellia terrane (Rioux *et al.*, 2007). Some Bonanza arc rocks show isotopic influence from their country rocks (older arc rocks along with some clastic sediments and carbonates), but many of the country rocks themselves are primitive isotopically (Samson *et al.*, 1990; Andrew *et al.*, 1991). A possible analogue to the SVF is the Salinian block (California, USA), where late Cretaceous granitoids intrude a thick sequence of sedimentary rock (Ducea *et al.*, 2003; Kidder *et al.*, 2003).

In the upper portions of the SVF arc section, which is dominated by tonalite and granodiorite, field and compositional evidence for the assimilation of country-rock by the SVF magmas is unequivocal (Otamendi *et al.*, 2009*a*, 2010*b*, 2012). In the mafic complex, sparse field relations clearly exhibit the process of country-rock melting and reaction (Otamendi *et al.*, 2008; Gallien *et al.*, 2010; Cristofolini *et al.*, 2012). Additionally, Ducea *et al.* (2010) reported the presence of xenocrystic zircons from one sample from the mafic zone. Finally, the radiogenic isotope compositions of the SVF rocks have a crustal component, with initial (475 Ma) $^{87}Sr/^{86}Sr > 0.7052$ and $\varepsilon_{Nd} < 2.1$, with most rocks having $Sr_i > 0.708$ and $\varepsilon_{Nd} < -4.0$ (Fig. 9; Otamendi *et al.*, 2012). Even the gabbronorites of the mafic zone have crustal isotopic signatures, although many are deficient in SiO_2 (<47%) and K_2O (<0·5%). This crustal isotopic affinity of the SVF rocks can plausibly be attributed in part to a 'polluted' mantle source in which the lithospheric mantle was already contaminated by crustal material, whether by lower crustal delamination, subduction erosion, or some other mechanism (Stern, 1991; Kay & Mahlburg Kay, 1993; Ducea & Saleeby, 1998; Lackey *et al.*, 2005). However, even with a contaminated mantle source some amount of crust is necessary to explain the

Table 7: Compositions of select amphibole grains from SVF rocks

Sample:	FA2-11-02	FA2-11-02	FA2-11-02	FA2-11-02	FA2-11-10	FA2-11-10	FA2-11-10	FA2-11-10
Lithology:	hbl gn	hbl gn	hbl gn	hbl gn	hbl gn	hbl gn	hbl gn	hbl gn
SiO_2	43·35	44·74	42·75	43·83	44·94	42·65	43·15	44·46
TiO_2	1·46	1·54	1·70	1·78	1·53	2·18	1·91	1·59
Al_2O_3	11·13	9·37	11·47	10·76	10·36	11·73	11·74	11·19
Cr_2O_3	0·04	0·02	0·02	0·00	0·02	0·04	0·02	0·00
FeO	14·16	14·90	14·54	14·21	11·60	12·60	12·22	11·13
MnO	0·18	0·27	0·16	0·21	0·16	0·14	0·13	0·12
MgO	12·49	12·45	12·36	12·67	14·63	13·28	13·33	14·26
CaO	11·62	11·48	11·19	11·78	11·76	11·80	11·96	12·07
Na_2O	1·37	1·27	0·98	1·34	1·56	1·72	1·69	1·52
K_2O	1·37	1·09	1·04	1·28	1·10	1·36	1·33	1·31
Total	97·17	97·13	96·21	97·86	97·66	97·51	97·48	97·65
Si	6·39	6·59	6·30	6·42	6·49	6·26	6·33	6·46
Al_{iv}	1·61	1·41	1·70	1·58	1·51	1·74	1·67	1·54
Al_{vi}	0·32	0·22	0·29	0·27	0·26	0·29	0·36	0·37
Ti	0·16	0·17	0·19	0·20	0·17	0·24	0·21	0·17
Cr	0·00	0·00	0·00	0·00	0·00	0·00	0·00	0·00
Fe^{3+}	0·64	0·65	1·04	0·60	0·63	0·51	0·40	0·40
Fe^{2+}	1·10	1·19	0·75	1·14	0·77	1·03	1·10	0·95
Mn	0·02	0·03	0·02	0·03	0·02	0·02	0·02	0·01
Mg	2·74	2·74	2·71	2·77	3·15	2·90	2·91	3·09
Ca	1·83	1·81	1·77	1·85	1·82	1·85	1·88	1·88
Na	0·39	0·36	0·28	0·38	0·44	0·49	0·48	0·43
K	0·26	0·21	0·20	0·24	0·20	0·26	0·25	0·24
Total	17·48	17·38	17·24	17·47	17·46	17·60	17·61	17·55
Na (B)	0·17	0·19	0·23	0·15	0·18	0·15	0·12	0·12
Ca (B)	1·83	1·81	1·77	1·85	1·82	1·85	1·88	1·88
(Na + K) (A)	0·48	0·38	0·24	0·47	0·46	0·60	0·61	0·55
$Mg/(Mg + Fe^{2+})$	0·71	0·70	0·78	0·71	0·80	0·74	0·73	0·76
Mg# (total Fe)	0·61	0·60	0·60	0·61	0·69	0·65	0·66	0·70
$Fe^{3+}/(Fe^{3+} + Al_{vi})$	0·67	0·74	0·78	0·69	0·71	0·64	0·53	0·52

Sample:	FA-09-16	FA-09-16	FA-09-16	FA-09-16	FA-10-19	FA-10-19	FA-10-19	FA-10-19
Lithology:	hbl gn	hbl gn	hbl gn	hbl gn	tonalite	tonalite	tonalite	tonalite
SiO_2	45·25	45·18	45·66	45·34	44·90	45·16	44·39	45·10
TiO_2	1·44	1·59	1·48	1·52	1·43	1·09	1·76	1·57
Al_2O_3	9·80	10·09	9·55	9·61	10·56	10·53	10·56	10·10
Cr_2O_3	0·10	0·17	0·14	0·11	0·08	0·15	0·23	0·10
FeO	12·79	12·23	11·92	12·03	12·93	12·42	12·92	12·57
MnO	0·17	0·10	0·12	0·09	0·16	0·11	0·17	0·14
MgO	13·92	14·11	14·38	14·26	13·43	14·02	13·28	13·61
CaO	11·98	11·93	12·08	12·03	11·78	11·65	11·71	11·76
Na_2O	1·33	1·36	1·26	1·38	0·97	0·99	1·09	0·94
K_2O	0·72	0·78	0·73	0·72	0·95	0·95	1·14	1·01
Total	97·51	97·52	97·31	97·10	97·19	97·08	97·25	96·90
Si	6·57	6·54	6·62	6·60	6·52	6·53	6·48	6·57
Al_{iv}	1·43	1·46	1·38	1·40	1·48	1·47	1·52	1·43
Al_{vi}	0·24	0·27	0·25	0·25	0·33	0·33	0·29	0·31
Ti	0·16	0·17	0·16	0·17	0·16	0·12	0·19	0·17
Cr	0·01	0·02	0·02	0·01	0·01	0·02	0·03	0·01
Fe^{3+}	0·63	0·59	0·54	0·53	0·70	0·82	0·63	0·64
Fe^{2+}	0·93	0·89	0·90	0·94	0·87	0·68	0·94	0·90
Mn	0·02	0·01	0·01	0·01	0·02	0·01	0·02	0·02
Mg	3·01	3·05	3·11	3·09	2·91	3·02	2·89	2·96
Ca	1·86	1·85	1·88	1·88	1·83	1·81	1·83	1·84
Na	0·37	0·38	0·35	0·39	0·27	0·28	0·31	0·26
K	0·13	0·14	0·13	0·13	0·18	0·18	0·21	0·19
Total	17·37	17·38	17·36	17·40	17·28	17·26	17·35	17·29
Na (B)	0·14	0·15	0·12	0·12	0·17	0·19	0·17	0·16
Ca (B)	1·86	1·85	1·88	1·88	1·83	1·81	1·83	1·84
(Na + K) (A)	0·37	0·38	0·36	0·40	0·28	0·26	0·35	0·29
$Mg/(Mg + Fe^{2+})$	0·76	0·77	0·78	0·77	0·77	0·82	0·75	0·77
Mg# (total Fe)	0·66	0·67	0·68	0·68	0·65	0·67	0·65	0·66
$Fe^{3+}/(Fe^{3+} + Al_{vi})$	0·72	0·69	0·68	0·68	0·68	0·72	0·68	0·67

Structural formula determined using cation charge summing to 46, and Fe^{2+}/Fe^{3+} estimated on the basis of 13 cations, after Leake *et al.* (1997).

Table 8: Compositions of selected plagioclase from SVF rocks

Sample:	FA-10-05	FA-10-05	FA-10-05	FA-11-12	FA-11-12	FA-11-12	FA2-11-10	FA2-11-10
Lithology:	tonalite	tonalite	tonalite	tonalite	tonalite	tonalite	hbl gn	hbl gn
SiO_2	54·97	55·66	56·50	55·70	54·52	52·64	46·19	45·71
Al_2O_3	28·70	27·99	27·68	27·90	28·55	29·95	34·59	34·37
FeO	0·05	0·11	0·18	0·02	0·09	0·08	0·14	0·89
CaO	10·87	10·38	9·46	10·36	11·34	12·71	17·50	17·68
SrO	0·01	0·08	0·05	0·08	0·08	0·08	0·04	0·03
Na_2O	5·24	5·45	5·69	5·82	5·31	4·47	1·50	1·26
K_2O	0·16	0·32	0·44	0·12	0·11	0·07	0·04	0·07
Total*	99·94	100·48	100·62	99·70	100·22	100·11	100·56	99·69
X_{An}	0·78	0·76	0·73	0·76	0·79	0·83	0·95	0·96
X_{Ab}	0·21	0·22	0·24	0·24	0·20	0·16	0·05	0·04

Sample:	FA-09-17	FA-09-17	FA2-11-02	FA2-11-02	FA-09-16	FA-09-16	FA-09-06	FA-09-06
Lithology:	amph–olv norite	amph–olv norite	hbl gn	hbl gn	hbl gn	hbl gn	hbl gn	hbl gn
SiO_2	43·83	44·67	50·28	53·19	46·68	45·38	45·19	45·63
Al_2O_3	35·74	35·19	31·73	29·52	34·10	34·93	34·61	34·43
FeO	0·10	0·11	0·20	0·13	0·21	0·17	0·21	0·59
CaO	19·47	18·78	14·34	12·29	17·22	18·21	18·46	17·75
SrO	0·06	0·08	0·02	0·06	0·05	0·05	0·03	0·07
Na_2O	0·79	1·14	3·29	4·61	1·70	1·23	1·48	1·51
K2O	0·02	0·04	0·13	0·21	0·04	0·03	0·02	0·03
Total*	99·93	99·95	99·98	100·16	100·41	100·14	99·84	99·68
X_{An}	0·98	0·97	0·88	0·82	0·95	0·96	0·96	0·95
X_{Ab}	0·02	0·03	0·11	0·17	0·05	0·04	0·04	0·04

*Pre-normalization totals.
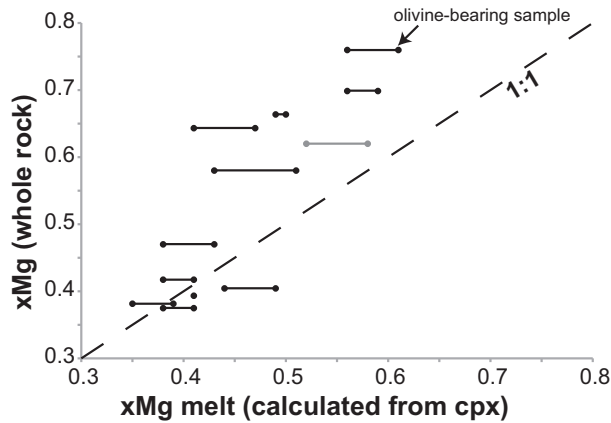
Fig. 11. Whole-rock X_{Mg} [Mg/(Mg + Fe$_{tot}$)] vs calculated melt X_{Mg} for mafic to ultramafic rocks in the Valle Fértil mafic zone. Melt X_{Mg} is calculated from clinopyroxene assuming a K_D^{cpx}(Fe–Mg) = 0·27 (Roeder & Emslie, 1970). Samples with whole-rock $X_{Mg} > 0.5$ have corresponding melt X_{Mg} values that are appreciably lower. This suggests that these rocks have accumulated Mg-bearing phases relative to the crystallizing magma. The range of melt X_{Mg} for single samples reflects multiple clinopyroxene analyses for each sample. One olivine-bearing sample is indicated, and the gray sample is from Otamendi *et al.* (2009*b*).

extreme isotopic variation of the SVF rocks (Otamendi *et al.*, 2012).

Despite field and isotopic evidence for crustal contributions within the mafic zone, major and trace element data are consistent with crystal fractionation alone (or rather, do not require the addition of a contaminant).

This presents a modeling dilemma because typical assimilation–fractional crystallization (AFC) models assume and predict coupled variations between elemental and isotopic compositions when mantle-derived magmas and crustal material are hybridized. With an increasing crustal isotopic signature, an increase in K_2O and SiO_2 and a decrease in CaO are expected. Crustal contamination is also expected to exert an influence on trace element concentrations, in particular incompatible elements such as Rb, Ba, Nb, and REE. As mentioned above, rocks from the SVF silicic and intermediate zones (above the mafic zone) preserve such elemental and isotopic coupling to some extent, and in particular display a high-K trend that is interpreted to be the product of assimilation and fractional crystallization. There are a few mafic zone tonalite samples that are compositionally suspect with respect to their major and trace elements (elevated K_2O, Rb and Ba; low CaO; presence of biotite; e.g. FA-09-23, FA-10-10, FA-11-19), but either these samples are near the top of the mafic section or the field relations demonstrate an intimate association with country-rock. Most mafic zone rocks—gabbronorites and tonalites alike—lack major and trace element crustal signatures. The mafic zone is largely devoid of elements that are incompatible in the plagioclase- and pyroxene-dominant assemblage.

We propose that elemental and isotopic decoupling can be understood as a product of time-transgressive assimilation, fractional crystallization, and melt loss in the lower crust. In the earliest stages of the SVF

Table 9: Fractional crystallization model for SVF mafic zone rocks (see text for details)

|	Parent	Cumulates					% Removed				
		1	2	3	4	5	0.2	0.15	0.1	0.3	0.3
SiO_2	50.9	44.6	48.9	45.8	44.0	49.9	52.5	53.2	54.0	58.3	61.9
TiO_2	0.807	0.20	0.52	0.97	1.38	1.31	0.96	1.04	1.04	0.90	0.72
Al_2O_3	17.18	17.66	18.08	17.56	17.79	18.61	17.06	16.88	16.81	16.38	15.43
FeO_t	10.53	9.05	9.29	13.08	15.66	12.40	10.90	11.18	10.97	8.95	7.48
MnO	0.242	0.14	0.19	0.24	0.25	0.24	0.27	0.28	0.28	0.30	0.33
MgO	7.48	15.93	8.96	8.18	6.80	5.05	5.37	4.74	4.35	3.30	2.55
CaO	10.44	11.63	12.49	12.53	12.37	9.44	10.15	9.73	9.42	8.16	7.61
Na_2O	1.88	0.61	1.16	1.23	1.33	2.36	2.20	2.39	2.51	3.02	3.31
K_2O	0.40	0.17	0.30	0.29	0.28	0.42	0.45	0.48	0.50	0.60	0.68
P_2O_5	0.095	0.03	0.07	0.11	0.19	0.28	0.11	0.12	0.12	0.09	0.01
X_{Mg}	0.56	0.76	0.63	0.53	0.44	0.42	0.51	0.49	0.48	0.50	0.54
Sc	35 (52)	30	43	51	51	39	58	60	61	66	77
V	267	99	217	370	495	289	310	326	321	246	228
Ba	90	56	63	71	71	141	99	105	109	125	118
Rb	4.50	4.7	6.5	4.1	4.1	7.9	4.4	4.1	4.1	4.1	2.4
Sr	190 (155)	155	167	188	199	231	199	204	206	209	200
Zr	65	19	27	34	38	171	76	85	91	114	89
Y	17 (31)	5	17	24	21	28	20	21	20	20	17
Nb	4.72	1.0	2.5	3.9	4.6	8.8	5.7	6.2	6.5	7.3	6.7
Ta	0.17	0.04	0.08	0.15	0.16	0.32	0.20	0.22	0.23	0.26	0.24
La	10 (13)	1.9	7.7	8.6	8.7	16.3	12.0	12.8	13.3	15.2	14.8
Ce	21 (30)	4.3	18.4	22.2	21.7	38.0	25.2	26.4	26.8	29.1	25.2
Pr	4.13	0.6	2.6	3.3	3.2	5.2	5.0	5.4	5.7	6.8	7.4
Nd	13 (18.5)	2.5	11.3	14.7	14.2	22.8	15.6	16.4	16.6	17.6	15.3
Sm	3 (5)	0.7	2.9	3.9	3.7	5.5	3.6	3.7	3.7	3.7	2.9
Eu	1.1 (1.3)	0.3	0.8	1.1	1.1	1.6	1.3	1.4	1.4	1.6	1.6
Gd	3.4 (5.5)	0.8	3.0	4.1	3.8	5.5	4.1	4.2	4.3	4.4	4.0
Tb	0.97	0.1	0.5	0.7	0.6	0.9	1.2	1.3	1.4	1.7	2.0
Dy	3.5 (6.2)	0.8	3.2	4.3	3.9	5.4	4.2	4.3	4.3	4.5	4.2
Ho	1.29	0.2	0.7	0.9	0.8	1.1	1.6	1.7	1.8	2.2	2.7
Er	3.52	0.5	1.9	2.4	2.2	2.9	4.3	4.7	4.9	6.1	7.5
Tm	0.51	0.1	0.3	0.3	0.3	0.4	0.6	0.7	0.7	0.9	1.1
Yb	1.6 (3.1)	0.4	1.8	2.2	1.9	2.5	1.9	1.9	1.9	1.9	1.6
Lu	0.25 (0.48)	0.1	0.3	0.3	0.3	0.4	0.6	0.6	0.7	0.8	1.0
U	0.25	0.11	0.12	0.09	0.09	0.22	0.29	0.32	0.35	0.46	0.55
Th	1.85	0.4	1.0	0.4	0.4	1.2	2.2	2.4	2.7	3.6	4.6
Hf	1.66	0.3	0.6	1.0	1.3	4.0	2.0	2.2	2.4	2.8	2.3

*Numbers in parentheses are actual calculated values. Numbers used in the model appear first.

magmatism when the thermal regime was relatively cool, and in areas where magma flux was low, any assimilation that occurred was incomplete and preserved in the mafic zone rocks (in both gabbronorites and tonalite). With continued mafic input, crustal melting was probably extensive, as expressed by large amounts of diatextite in neighboring septa, but the high temperature and increasingly mafic-dominated compositions would limit the stability of minerals that partition crustally contributed, incompatible major and trace elements (Barnes, 1986; Reiners *et al.*, 1995). Prolonged or punctuated periods of magma injection, crystallization, assimilation, and melt segregation would thus result in crustally contributed major and trace elements being exported from the mafic zone. Throughout this process, however, mineral accumulation would preserve crustally derived isotopic signatures—the only detectable evidence of the assimilant. Elemental and isotopic decoupling, then, is conceivably an expected by-product of prolonged mafic magmatism involving assimilation accompanied by extremely efficient crystal–melt segregation.

The anatomy of a MASH zone revealed

We interpret the mafic zone as the site at which mafic magmas stalled, assimilated crust, partially crystallized and remobilized previously stalled magmas. Such a scenario is consistent with the MASH process (melting, assimilation, storage, homogenization) proposed by Hildreth & Moorbath (1988). We document such a process from a field-based geological perspective. Although assimilation and crystallization probably occurred at multiple levels within the SVF system, the mafic zone probably represents the first and perhaps principal stage of differentiation of mantle-derived melts prior to subsequent reintrusion or eruption. The most primitive components are preserved as ultramafic cumulates that occur sporadically throughout the mafic section, forming discrete bodies that range in size from tens of meters to ~400 m thick (by <1 km wide). We interpret the dimensions of these ultramafic bodies as indicative of the size of possible parental magma batches at this level of the system (actual batch sizes must have been much larger as these ultramafic cumulates are interpreted to have lost ~80% melt). Although not
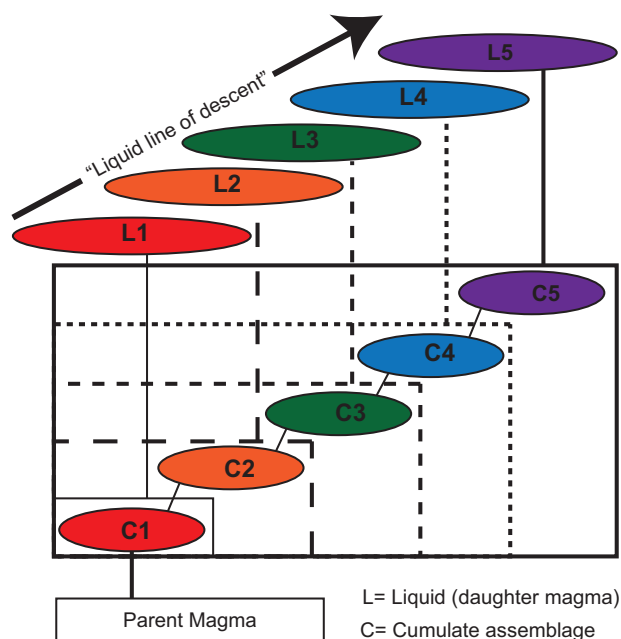
Fig. 12. Schematic diagram of the fractionation model. From a parent magma, a cumulate assemblage (C1) is subtracted and a daughter liquid (L1) is produced. From the L1 daughter liquid, a second cumulate (C2) is subtracted and a second daughter liquid (L2) is produced. From that L2 liquid, a third cumulate (C3) is subtracted, yielding a third daughter liquid (L3), and so on. In the diagram, daughter liquids are connected by patterned lines with their total crystal residues, which are enclosed by a box with the same pattern. For example, the daughter magma L1 has the crystal residue of C1. So, L1 + C1 = parent magma. However, the crystal residue of the daughter magma L4 includes C1, C2, C3, and C4. Therefore, L4 + C1 + C2 + C3 + C4 = parent magma.

representing the amount of molten material at any given moment, the ultramafic cumulates, nonetheless, might indicate the relative volumes of magmatic pulses in pluton-building episodes. The gabbronorites, then, must represent residual compositions after repeated magma injection, back-mixing, fractionation and melt expulsion. Tonalites represent melts that were separated from these gabbronorite cumulate assemblages.

This simplified framework of cumulates and segregated melt produces very complex field relationships. In the field, samples were selected from relatively homogeneous domains (or at least portions of outcrop). However, many of the outcrops we observe in the SVF mafic zone are extremely heterogeneous (including multiple generations of enclaves, some with cumulate compositions) and lack visible contacts between modally distinct domains. The internal organization of the mafic zone seems to reflect a prolonged, chaotic assembly process. Mafic magmas intruded variably cumulate tonalites, tonalite magmas intruded variably cumulate gabbronorites, and these processes occurred both high and low within the mafic zone. Gradational contacts between different gabbroic and tonalitic rocks suggest that re-intrusion blended existing cumulates with new intrusions and involved near-simultaneous melt extraction.

In general, field relations in the SVF mafic zone share some features with those described at the Onion Valley sill complex in the Sierra Nevada (Sisson *et al.*, 1996). The Onion Valley complex is composed of basaltic to basaltic andesite sills that intruded an existing granodiorite matrix. The sills are of variable thickness and include multiply injected swarm complexes, some of which contain olivine, are modally layered, and are interpreted as cumulates. However, owing in part to their shallow emplacement depth (~2 kbar pressure), the Onion Valley sills have several characteristics that the SVF mafic magmas lack. In particular, the Onion Valley sills have chilled margins and miarolitic cavities; many are interpreted to preserve melt compositions (Sisson *et al.*, 1996). However, the general interpretation that the mafic sills invaded a solid to partially molten silicic crystal mush is consistent with our observations for the SVF. In the SVF the invading mafic sills were emplaced into, and fractionated within, tonalites that are themselves products of the same process (Fig. 15). The SVF mafic complex also shares features with the Woolley Creek batholith of the Klamath Mountains, California, with the important exception that at Woolley Creek there was not as much homogenization between new magma batches as observed at SVF (Coint *et al.*, 2013).

Discrete compositional domains persisted in the SVF mafic complex, despite prolonged, open-system mush-blending; however, compositional variation is present within single domains. For example, any given 'gabbronorite' domain on the map (Fig. 16) contains a spectrum of compositions. Additionally, specific compositional varieties (of gabbronorite or tonalite) are not spatially confined, but are found seemingly randomly distributed within the mafic zone. Although our petrogenetic model is consistent with a residue-segregated melt relationship for the gabbronorites and tonalites the actual process is almost certainly much more complex. Tonalites and gabbronorites are probably composed of melt–mineral combinations that, although roughly appearing to be an equilibrium assemblage, may in fact be hybrids. Fractional crystallization is plausibly the dominant mechanism responsible for compositional variation, but compositional trends are also probably in part due to back-mixing, incomplete melt extraction and melt re-infiltration.

CONCLUSIONS

The SVF mafic zone represents the upper part of a MASH zone in which mafic, mantle-derived magmas penetrated the crust. The compositional spectrum of SVF mafic zone rocks is consistent with a crystal fractionation process in which the mafic to ultramafic rocks—mostly various types of gabbronorite—are cumulates, and the tonalites are the corresponding silicic segregates. It is clear from the Sr and Nd isotope data that assimilation of crustal rocks occurred at all levels within the SVF system, and possibly also within the mantle wedge. Major and trace element evidence for
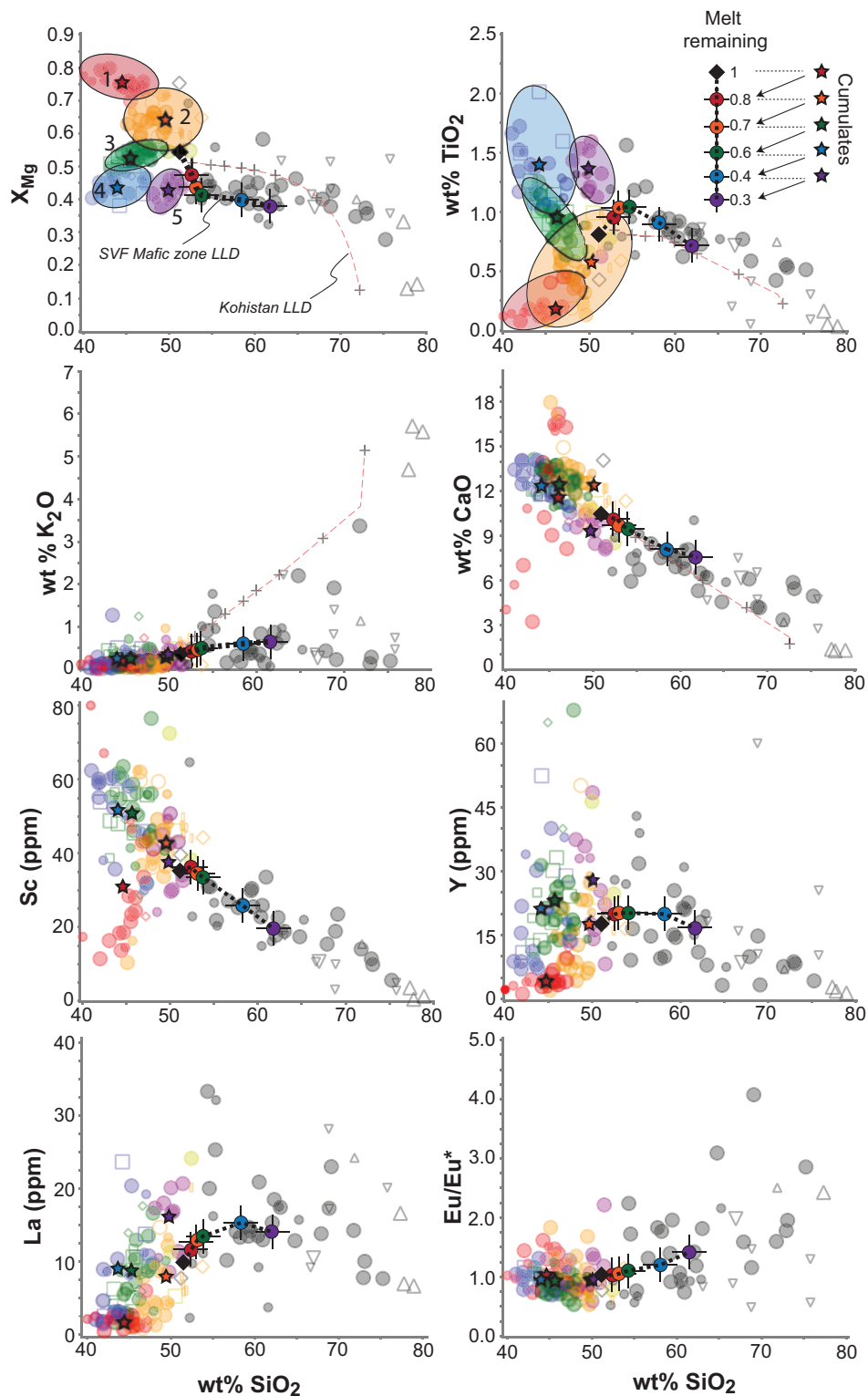
Fig. 13. Variation of selected elements vs SiO_2 and the fractional crystallization model for the SVF mafic zone rocks. The starting composition is indicated by a black diamond. Model cumulate assemblages are indicated by stars and are the calculated averages of the translucent data points of the same color (cumulate groups used for averaging are circled in plots of X_{Mg} and TiO_2). From the starting composition, the cumulates are progressively subtracted in the order 1–5 (labeled in the X_{Mg} and TiO_2 vs SiO_2 plots). Bold colored circles with crosses are the modeled daughter magma compositions, the color of which corresponds to the cumulate assemblage subtracted during its fractionation step. The melt remaining (F) at each interval of fractionation is indicated. Modeled liquid lines of descent for selected elements from the Kohistan arc system are also shown (Jagoutz, 2010). In general, there is good agreement between our model liquid lines of descent and those of Jagoutz (2010), with the notable exception of K_2O. (See text for additional details of our model.) $X_{Mg} = Mg/(Mg + Fe_{tot})$. LLD, liquid line of descent.
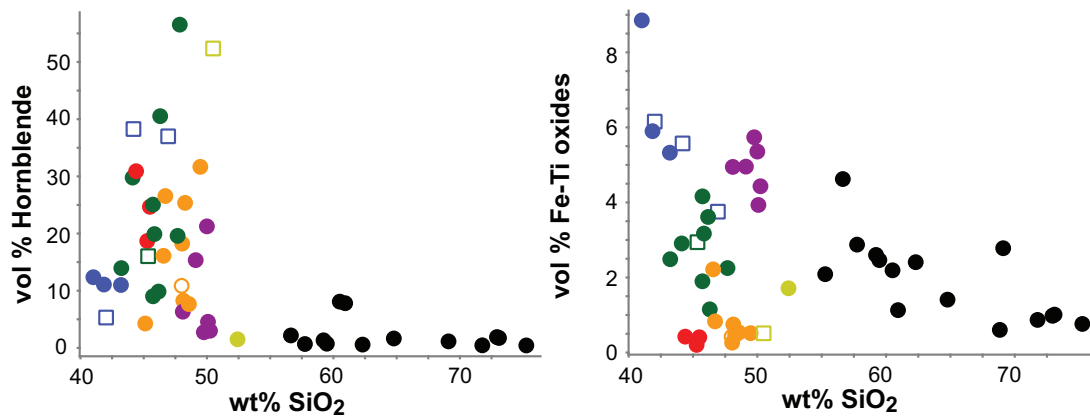
Fig. 14. Amphibole (hornblende) and Fe–Ti oxides (magnetite and ilmenite) modes vs weight per cent SiO$_2$ for the SVF mafic zone rocks. It should be noted that the rocks with lowest SiO$_2$ are those with the highest volume per cent Fe–Ti oxides. Symbols are as in Fig. 6. Open squares, dikes; open circles, blob-like inclusions.
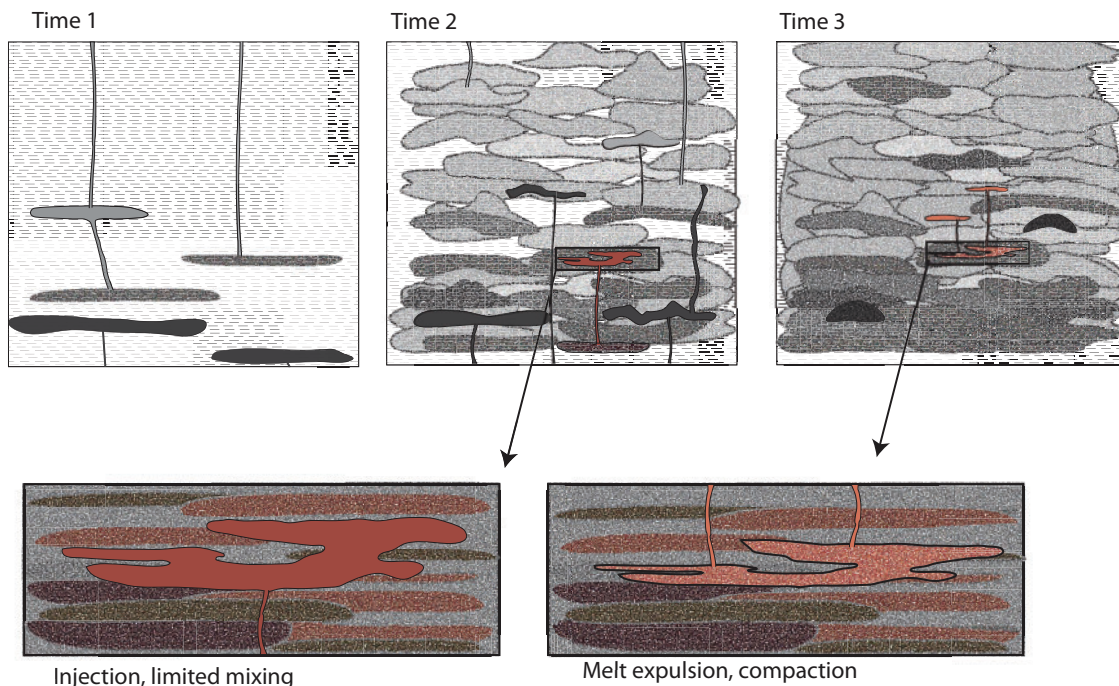
Fig. 15. Schematic illustration of generalized assembly of the Sierra Valle Fértil mafic zone. A prolonged, chaotic scenario involving MASH-like processes is envisioned. Efficient melt extraction leaves behind distinct cumulate packages, but thermal annealing probably obscures initial intrusion and extraction contacts. Discrete compositional domains persist, although these domains themselves appear to comprise multiple sheets of distinct composition.

assimilation is sparse within the mafic zone rocks, suggesting that the incompatible components of the assimilated crust were flushed out with extraordinary efficiency during prolonged magmatism. The silicic liquid extracted from the MASH zone was expelled upward in the system, giving rise to compositionally stratified arc crust almost completely reconstituted by magmatism. Despite a large-scale stratification consisting of a mafic deep crust, intermediate mid-crust and silicic upper crust (Otamendi *et al.*, 2012), the SVF mafic complex is characterized by considerable heterogeneity at smaller scales. This is indicative of very complex temporal and spatial assembly processes, all sharing a common thermal environment at the prograde peak. Models for arc processes that invoke a 'ball and stick' morphology—where the mid-crust is transparent to the petrogenetic processes, and evolved magmas leave the deep crust and rise superheated to the upper crust—are not supported by this field example. It is also worth restating that there is no field evidence for the production of voluminous silicic magmas by simple melting of mafic precursors; the mid-crustal intermediate magmas
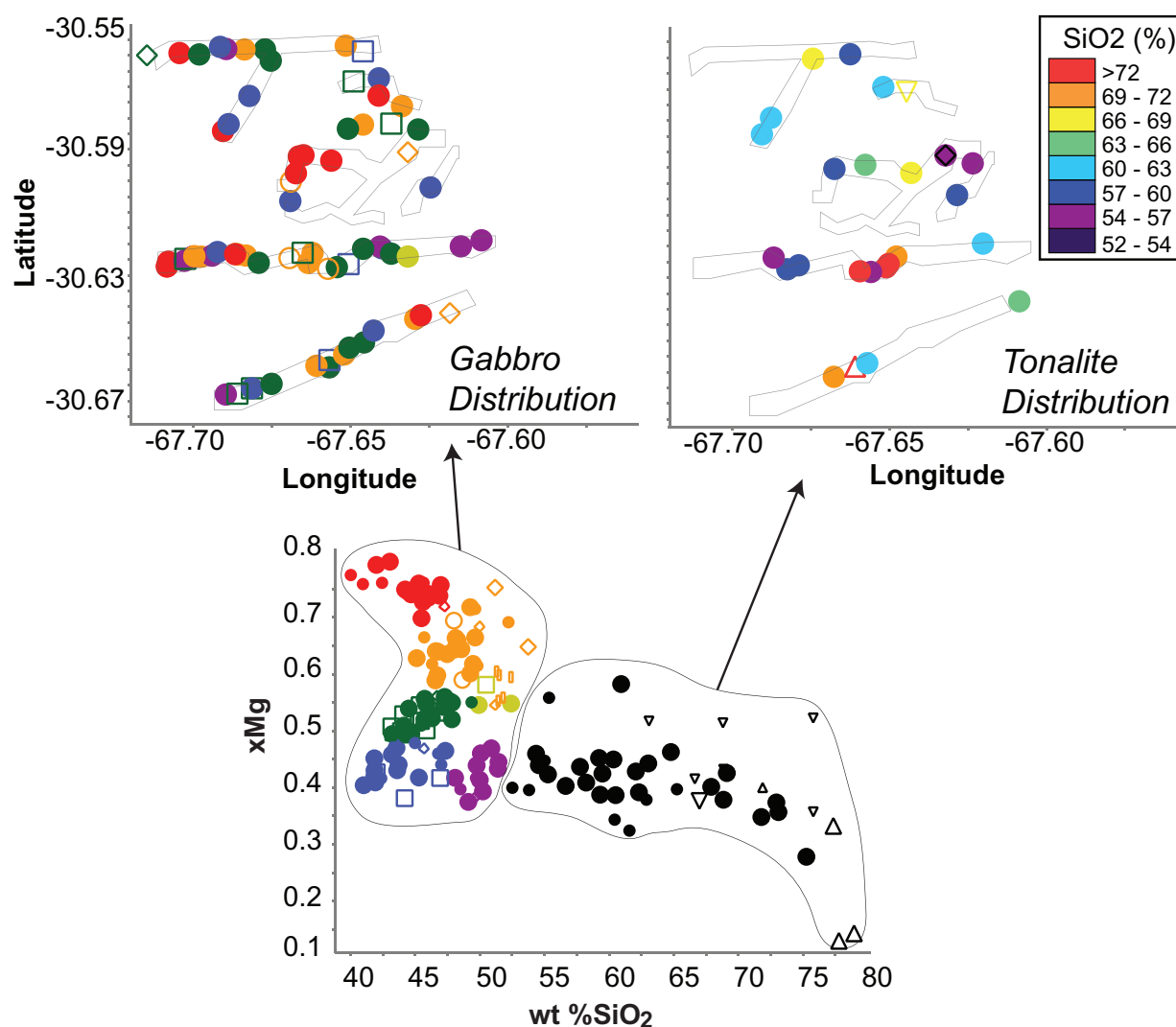
Fig. 16. Spatial distributions (latitude–longitude) of compositional variants of gabbro and tonalite in the SVF mafic zone. Gabbroic rocks are plotted with respect to their latitude–longitude, color-coded according to their position in the X_{Mg} vs SiO_2 plot. Tonalites, shown in black on the X_{Mg} vs SiO_2 plot, are color coded based on their SiO_2 content in the latitude–longitude plot. Outlines of canyons are from Fig. 2.

at the SVF appear to be the product of crystal fractionation and some assimilation.

SUPPLEMENTARY DATA

Supplementary data for this paper are available at *Journal of Petrology* online.

REFERENCES

Acenolaza, F. G., Miller, H. & Toselli, A. J. (2002). Proterozoic–Early Paleozoic evolution in western South America—a discussion. *Tectonophysics* **354**, 121–137.

Andrew, A., Armstrong, R. L. & Runkle, D. (1991). Neodymium–strontium–lead isotopic study of Vancouver Island igneous rocks. *Canadian Journal of Earth Sciences* **28**, 1744–1752.

Annen, C., Blundy, J. D. & Sparks, R. S. J. (2006). The genesis of intermediate and silicic magmas in deep crustal hot zones. *Journal of Petrology* **47**, 505–539.

Bachl, C. A., Miller, C. F., Miller, J. S. & Faulds, J. E. (2001). Construction of a pluton: Evidence from an exposed cross section of the Searchlight pluton, Eldorado Mountains, Nevada. *Geological Society of America Bulletin* **113**, 1213–1228.

Barboza, S. A. & Bergantz, G. W. (1996). Dynamic model of dehydration melting motivated by a natural analogue: applications to the Ivrea–Verbano zone, northern Italy. *Transactions of the Royal Society of Edinburgh* **87**, 23–31.

Barboza, S. A. & Bergantz, G. W. (2000). Metamorphism and anatexis in the mafic complex contact aureole, Ivrea Zone, Northern Italy. *Journal of Petrology* **41**, 1307–1327.

Barnes, S. (1986). The effect of trapped liquid crystallization on cumulus mineral compositions in layered intrusions. *Contributions to Mineralogy and Petrology* **93**, 524–531.

Beard, J. S. (1995). Experimental, geological, and geochemical constraints on the origins of low-K silicic magmas in oceanic arcs. *Journal of Geophysical Research: Solid Earth* **100**, 15593–15600.

Beard, J. S. (1997). Geochemistry and petrogenesis of tonalite dikes in the Smith River allochthon, south–central Virginia. In: Sinha, A.K, Whalen, J.B., Hogan, J.P., (eds) *The Nature of Magmatism in the Appalachian Orogen. Geological Society of America, Memoirs* **191**, 75–86.

Beard, J. S. & Lofgren, G. E. (1989). Effects of water on the composition of partial melts of greenstone and amphibolite. *Science* **244**, 195–197.

Bergantz, G. W. (1991). Physical and chemical characterization of plutons. In: Kerrick, D. M. (ed.) *Contact Metamorphism. Mineralogical Society of America, Reviews in Mineralogy* **26**, 13–42.

Bergantz, G. W. (1992). Conjugate solidification and melting in multicomponent open and closed systems. *International Journal of Heat and Mass Transfer* **35**, 533–543.

Bucholz, C., Jagoutz, O., Schmidt, M. & Sambuu, O. (2014). Fractional crystallization of high-K arc magmas: biotite- versus amphibole-dominated fractionation series in the Dariv Igneous Complex, Western Mongolia. *Contributions to Mineralogy and Petrology* **168**, 1–28.

Burg, J. P., Bodinier, J. L., Chaudhry, S., Hussain, S. & Dawood, H. (1998). Infra-arc mantle–crust transition and intra-arc mantle diapirs in the Kohistan Complex (Pakistani Himalaya): petro-structural evidence. *Terra Nova* **10**, 74–80.

Calvert, A. J., Klemperer, S. L., Takahashi, N. & Kerr, B. C. (2008). Three-dimensional crustal structure of the Mariana island arc from seismic tomography. *Journal of Geophysical Research: Solid Earth* **113** doi: 10.1029/2007JB004939.

Casquet, C., Rapela, C. W., Pankhurst, R. J., Baldo, E., Galindo, C., Fanning, C. M. & Dahlquist, J. (2012). Fast sediment underplating and essentially coeval juvenile magmatism in the Ordovician margin of Gondwana, Western Sierras Pampeanas, Argentina. *Gondwana Research* **22**, 664–673.

Claeson, D. & Meurer, W. (2004). Fractional crystallization of hydrous basaltic 'arc-type' magmas and the formation of amphibole-bearing gabbroic cumulates. *Contributions to Mineralogy and Petrology* **147**, 288–304.

Claiborne, L. L., Miller, C. F., Walker, B. A., Wooden, J. L., Mazdab, F. K. & Bea, F. (2006). Tracking magmatic processes through Zr/Hf ratios in rocks and Hf and Ti zoning in zircons: An example from the Spirit Mountain batholith, Nevada. *Mineralogical Magazine* **70**, 517–543.

Clemens, J. D., Stevens, G. & Farina, F. (2011). The enigmatic sources of I-type granites: The peritectic connexion. *Lithos* **126**, 174–181.

Coint, N., Barnes, C. G., Yoshinobu, A. S., Chamberlain, K. R. & Barnes, M. A. (2013). Batch-wise assembly and zoning of a tilted calc-alkaline batholith: Field relations, timing, and compositional variation. *Geosphere* **9**, 1729–1746.

Coleman, D. S., Bartley, J. M., Glazner, A. F. & Pardue, M. J. (2012). Is chemical zonation in plutonic rocks driven by changes in source magma composition or shallow-crustal differentiation? *Geosphere* **8**, 1568–1587.

Collo, G., Astini, R. A., Cawood, P. A., Buchan, C. & Pimentel, M. (2009). U–Pb detrital zircon ages and Sm–Nd isotopic features in low-grade metasedimentary rocks of the Famatina belt: implications for late Neoproterozoic–early Palaeozoic evolution of the proto-Andean margin of Gondwana. *Journal of the Geological Society, London* **166**, 303–319.

Conrad, W. K. & Kay, R. W. (1984). Ultramafic and mafic inclusions from Adak Island—crystallization history, and implications for the nature of primary magmas and crustal evolution in the Aleutian Arc. *Journal of Petrology* **25**, 88–125.

Cristofolini, E. A., Otamendi, J. E., Ducea, M. N., Pearson, D. M., Tibaldi, A. M. & Baliani, I. (2012). Detrital zircon U–Pb ages of metasedimentary rocks from Sierra de Valle Fértil: Entrapment of Middle and Late Cambrian marine successions in the deep roots of the Early Ordovician Famatinian arc. *Journal of South American Earth Sciences* **37**, 77–94.

Cristofolini, E. A., Otamendi, J. E., Walker, B. A., Jr, Tibaldi, A. M., Armas, P., Bergantz, G. W. & Martino, R. D. (2014). A Middle Paleozoic shear zone in the Sierra de Valle Fértil, Argentina: Records of a continent–arc collision in the Famatinian margin of Gondwana. *Journal of South American Earth Sciences* **56**, 170–185.

Cui, Y. & Russell, J. K. (1995). Nd–Sr–Pb isotopic studies of the southern Coast Plutonic Complex, southwestern British Columbia. *Geological Society of America Bulletin* **107**, 127–138.

Davidson, J., Turner, S., Handley, H., Macpherson, C. & Dosseto, A. (2007). Amphibole 'sponge' in arc crust? *Geology* **35**, 787–790.

DeBari, S. M. (1994). Petrogenesis of the Fimbala gabbroic intrusion, northwestern Argentina, a deep crustal syntectonic pluton in a continental magmatic arc. *Journal of Petrology* **35**, 679–713.

DeBari, S. M. & Coleman, R. G. (1989). Examination of the deep levels of an island arc: Evidence from the Tonsina Ultramafic–Mafic Assemblage, Tonsina, Alaska. *Journal of Geophysical Research: Solid Earth* **94**, 4373–4391.

DeBari, S. M. & Mortensen, J. (1994). The Jurassic Bonanza arc, Vancouver Island, Canada: A window into the deep crust of an island arc. *Geological Society of America, Abstracts with Programs, Annual Meeting* A-332.

DeBari, S. M., Anderson, R. G. & Mortensen, J. K. (1999). Correlation among lower to upper crustal components in an island arc: the Jurassic Bonanza arc, Vancouver Island, Canada. *Canadian Journal of Earth Sciences* **36**, 1371–1413.

Dessimoz, M., Muntener, O. & Ulmer, P. (2012). A case for hornblende dominated fractionation of arc magmas: the Chelan Complex (Washington Cascades). *Contributions to Mineralogy and Petrology* **163**, 567–589.

Dhuime, B., Bosch, D., Garrido, C. J., Bodinier, J.-L., Bruguier, O., Hussain, S. S. & Dawood, H. (2009). Geochemical architecture of the lower- to middle-crustal section of a paleo-island arc (Kohistan complex, Jijal–Kamila area, northern Pakistan): implications for the evolution of an oceanic subduction zone. *Journal of Petrology* **50**, 531–569.

Dilles, J. H. (1987). Petrology of the Yerington Batholith, Nevada—evidence for evolution of porphyry copper ore fluids. *Economic Geology* **82**, 1750–1789.

Ducea, M. N. & Saleeby, J. (1998). The age and origin of a thick mafic–ultramafic root from beneath the Sierra Nevada batholith. *Contributions to Mineralogy and Petrology* **133**, 169–185.

Ducea, M. N., Kidder, S. & Zandt, G. (2003). Arc composition at mid-crustal depths: insights from the Coast Ridge Belt, Santa Lucia Mountains, California. *Geophysical Research Letters* **30**, 1703–1706.

Ducea, M. N., Otamendi, J. E., Bergantz, G., Stair, K. M., Valencia, V. A. & Gehrels, G. E. (2010). Timing constraints on building an intermediate plutonic arc crustal section: U–Pb zircon geochronology of the Sierra Valle Fertil–La Huerta, Famatinian arc, Argentina. *Tectonics* **29** doi: 10.1029/2009TC002615.

Ducea, M. N., Otamendi, J. E., Bergantz, G. W., Jianu, D. & Petrescu, L. (2014). The origin and petrologic evolution of the Ordovician Famatinian–Puna arc. In: DeCelles, P.G. et al (eds) *Geodynamics of a Cordilleran Orogenic System: The Central Andes of Argentina and Northern Chile. Geological Society of America, Memoirs* **212**, 125–138.

Ducea, M. N., Saleeby, J. B. & Bergantz, G. (2015). The architecture, chemistry, and evolution of continental magmatic arcs. *Annual Review of Earth and Planetary Sciences* **43**, 299–331.

Dufek, J. & Bergantz, G. W. (2005). Lower crustal magma genesis and preservation: a stochastic framework for the evaluation of basalt–crust interaction. *Journal of Petrology* **46**, 2167–2196.

Economos, R. C., Hanzl, P., Hrdlickova, K., Burianek, D., Said, L. O., Gerdes, A. & Paterson, S. R. (2008). Geochemical and structural constraints on the magmatic history of the Chandman Massif of the eastern Mongolian Altay Range, SW Mongolia. *Journal of Geosciences* **53**, 335–352.

Gallien, F., Mogessie, A., Bjerg, E., Delpino, S., de Machuca, B. C., Thöni, M. & Klötzli, U. (2010). Timing and rate of granulite facies metamorphism and cooling from multi-mineral chronology on migmatitic gneisses, Sierras de La Huerta and Valle Fértil, NW Argentina. *Lithos* **114**, 229–252.

Greene, A. R., DeBari, S. M., Kelemen, P. K., Blustajn, J. & Clift, P. D. (2006). A detailed geochemical study of island arc crust: the Talkeetna arc section, south–central Alaska. *Journal of Petrology* **47**, 1051–1093.

Hacker, B. R., Mehl, L., Kelemen, P. B., Rioux, M., Behn, M. D. & Luffi, P. (2008). Reconstruction of the Talkeetna intraoceanic arc of Alaska through thermobarometry. *Journal of Geophysical Research: Solid Earth* **113 22** doi:10.1029/2007JB005208.

Haraguchi, S., Ishii, T., Kimura, J.-I. & Ohara, Y. (2003). Formation of tonalite from basaltic magma at the Komahashi–Daini Seamount, northern Kyushu–Palau Ridge in the Philippine Sea, and growth of Izu–Ogasawara (Bonin)–Mariana arc crust. *Contributions to Mineralogy and Petrology* **145**, 151–168.

Hildreth, W. (1981). Gradients in silicic magma chambers: implications for lithospheric magmatism. *Journal of Geophysical Reserach* **86**, 10153–110192.

Hildreth, W. & Moorbath, S. (1988). Crustal contributions to arc magmatism in the Andes of Central Chile. *Contributions to Mineralogy and Petrology* **98**, 455–489.

Hoal, K. O., Stammer, J. G., Appleby, S. K., Botha, J., Ross, J. K. & Botha, P. W. (2009). Research in quantitative mineralogy: Examples from diverse applications. *Minerals Engineering* **22**, 402–408.

Holbrook, W. S., Lizarralde, D., McGeary, S., Bangs, N. & Diebold, J. (1999). Structure and composition of the Aleutian island arc and implications for continental crustal growth. *Geology* **27**, 31–34.

Hoskin, P. W. O. & Schaltegger, U. (2003). The composition of zircon and igneous and metamorphic petrogenesis. In: Hanchar, J. M. & Hoskin, P. W. O. (eds) *Zircon. Mineralogical Society of America and Geochemical Society, Reviews in Mineralogy and Geochemistry* **53**, 27–62.

Jagoutz, O. (2010). Construction of the granitoid crust of an island arc. Part II: a quantitative petrogenetic model. *Contributions to Mineralogy and Petrology* **160**, 359–381.

Jagoutz, O., Müntener, O., Burg, J. P., Ulmer, P. & Jagoutz, E. (2006). Lower continental crust formation through focused flow in km-scale melt conduits: The zoned ultramafic bodies of the Chilas Complex in the Kohistan island arc (NW Pakistan). *Earth and Planetary Science Letters* **242**, 320–342.

Jagoutz, O., Muntener, O., Ulmer, P., Pettke, T., Burg, J.-P., Dawood, H. & Hussain, S. (2007). Petrology and mineral chemistry of lower crustal intrusions: the Chilas Complex, Kohistan (NW Pakistan). *Journal of Petrology* **48**, 1895–1953.

Jagoutz, O., Müntener, O., Schmidt, M. W. & Burg, J.-P. (2011). The roles of flux- and decompression melting and their respective fractionation lines for continental crust formation: Evidence from the Kohistan arc. *Earth and Planetary Science Letters* **303**, 25–36.

Johnson, D. M., Hooper, P. R. & Conrey, R. M. (1999). XRF analysis of rocks and minerals for major and trace elements on a single low dilution Li-tetraborate fused bead. *Advances in X-ray Analysis* **41**, 843–867.

Kamiyama, H., Nakajima, T. & Kamioka, H. (2007). Magmatic stratigraphy of the tilted Tottabetsu plutonic complex, Hokkaido, North Japan: Magma chamber dynamics and pluton construction. *Journal of Geology* **115**, 295–314.

Kawate, S. & Arima, M. (1998). Petrogenesis of the Tanzawa plutonic complex, central Japan: exposed felsic mid-crust of the Izu–Bonin–Mariana arc. *Island Arc* **7**, 342–358.

Kay, R. W. & Mahlburg Kay, S. (1993). Delamination and delamination magmatism. *Tectonophysics* **219**, 177–189.

Kidder, S., Ducea, M., Gehrels, G., Patchett, P. J. & Vervoot, J. (2003). Tectonic and magmatic development of the Salinian Coast Ridge belt. *Tectonics* **22** doi:10.1029/2002TC001409.

Kitamura, K., Ishikawa, M. & Arima, M. (2003). Petrological model of the northern Izu–Bonin–Mariana arc crust: constraints from high-pressure measurements of elastic wave velocities of the Tanzawa plutonic rocks, central Japan. *Tectonophysics* **371**, 213–221.

Lackey, J. S., Valley, J. W. & Saleeby, J. B. (2005). Supracrustal input to magmas in the deep crust of Sierra Nevada batholith: Evidence from high-δ^{18}O zircon. *Earth and Planetary Science Letters* **235**, 315–330.

Larocque, J. & Canil, D. (2010). The role of amphibole in the evolution of arc magmas and crust: the case from the Jurassic Bonanza arc section, Vancouver Island, Canada. *Contributions to Mineralogy and Petrology* **159**, 475–492.

Leake, B. E., Woolley, A. R., Arps, C. E. S., Birch, W. D., Gilbert, M. C., Grice, J. D., Hawthorne, F. C., Kato, A., Kisch, H. J., Krivovichev, V. G., Linthout, K., Laird, J., Mandarino, J. A., Maresch, W. V., Nickel, E. H., Rock, N. M. S., Schumacher, J. C., Smith, D. C., Stephenson, N. C. N., Ungaretti, L., Whittaker, E. J. W. & Guo, Y. (1997). Nomenclature of amphiboles; Report of the Subcommittee on Amphiboles of the International Mineralogical Association, Commission on New Minerals and Mineral Names. *American Mineralogist* **82**, 1019–1037.

Lee, C. T., Rudnick, R. L. & Brimhall, G. H. (2001). Deep lithospheric dynamics beneath the Sierra Nevada during the Mesozoic and Cenozoic as inferred from xenolith petrology.

Geochemistry, Geophysics, Geosystems **2** doi:10.1029/2001GC000152.

Longo, A. A., Dilles, J. H., Grunder, A. L. & Duncan, R. (2010). Evolution of calc-alkaline volcanism and associated hydrothermal gold deposits at Yanacocha, Peru. *Economic Geology* **105**, 1191–1240.

Meurer, W. P. & Claeson, D. T. (2002). Evolution of crystallizing interstitial liquid in an arc-related cumulate determined by LA ICP-MS mapping of a large amphibole oikocryst. *Journal of Petrology* **43**, 607–629.

Miller, C. F. & Miller, J. S. (2002). Contrasting stratified plutons exposed in tilt blocks, Eldorado Mountains, Colorado River Rift, NV, USA. *Lithos* **61**, 209–224.

Miller, R. B. & Paterson, S. R. (2001). Construction of mid-crustal sheeted plutons: Examples from the north Cascades, Washington. *Geological Society of America Bulletin* **113**, 1423–1442.

Miller, R. B., Paterson, S. R. & Matzel, J. P. (2009). Plutonism at different crustal levels: Insights from the ∼5–40 km (paleodepth) North Cascades crustal section, Washington. In: Miller, R. B. & Snoke, A.W. (eds) *Crustal Cross Sections from the Western North American Cordillera and Elsewhere: Implications for Tectonic and Petrologic Processes. Geological Society of America, Special Papers* **456**, 125–149.

Mirré, J. C. (1976). *Descripción Geológica de la Hoja 19e, Valle Fértil, Provincias de San Juan y La Rioja*. Servicio Geológico Nacional, pp. 1–70.

Mulcahy, S. R., Roeske, S. M., McClelland, W. C., Nomade, S. & Renne, P. R. (2007). Cambrian initiation of the Las Piquitas thrust of the western Sierras Pampeanas, Argentina: Implications for the tectonic evolution of the proto-Andean margin of South America. *Geology* **35**, 443–446.

Mulcahy, S. R., Roeske, S. M., McClelland, W. C., Ellis, J. R., Jourdan, F., Renne, P. R., Vervoort, J. D. & Vujovich, G. I. (2014). Multiple migmatite events and cooling from granulite facies metamorphism within the Famatina arc margin of northwest Argentina. *Tectonics* **33**, 1–25.

Needy, S. K., Anderson, J. L., Wooden, J. L., Fleck, R. J., Barth, A. P., Paterson, S. R., Memeti, V. & Pignotta, G. S. (2009). Mesozoic magmatism in an upper- to middle-crustal section through the Cordilleran continental margin arc, eastern Transverse Ranges, California. In: Miller, R. B. & Snoke, A.W. (eds) *Crustal Cross Sections from the Western North American Cordillera and Elsewhere: Implications for Tectonic and Petrologic Processes. Geological Society of America, Special Papers* **456**, 187–218.

Nui, Y., Gilmore, T., Mackie, S., Greig, A. & Bach, W. (2002). Mineral chemistry, whole-rock compositions, and petrogenesis of Leg 176 gabbros: data and discussion. In: Natland, J.H., Dick, H.J.B., Miller, D.J. & Von Herzen, R.P. (eds) *Proc. ODP, Sci. Results*, **176**, 1–60.

Otamendi, J. E., Tibaldi, A. M., Vujovich, G. I. & Viñao, G. A. (2008). Metamorphic evolution of migmatites from the deep Famatinian arc crust exposed in Sierras Valle Fértil–La Huerta, San Juan, Argentina. *Journal of South American Earth Sciences* **25**, 313–335.

Otamendi, J. E., Ducea, M., Tibaldi, A. M., Bergantz, G. W., de la Rosa, J. D. & Vujovich, G. I. (2009a). Generation of tonalitic and dioritic magmas by coupled partial melting of gabbroic and metasedimentary rocks within the deep crust of the Famatinian magmatic arc, Argentina. *Journal of Petrology* **50**, 841–873.

Otamendi, J. E., Vujovich, G. I., de la Rosa, J. D., Tibaldi, A. M., Castro, A., Martino, R. D. & Pinotti, L. P. (2009b). Geology and petrology of a deep crustal zone from the Famatinian paleo-arc, Sierras de Valle Fertil and La Huerta, San Juan, Argentina. *Journal of South American Earth Sciences* **27**, 258–279.

Otamendi, J. E., Cristofolini, E., Tibaldi, A. M., Quevedo, F. I. & Baliani, I. (2010a). Petrology of mafic and ultramafic layered rocks from the Jaboncillo Valley, Sierra de Valle Fértil, Argentina: Implications for the evolution of magmas in the lower crust of the Famatinian arc. *Journal of South American Earth Sciences* **29**, 685–704.

Otamendi, J. E., Pinotti, L. P., Basei, M. A. S. & Tibaldi, A. M. (2010b). Evaluation of petrogenetic models for intermediate and silicic plutonic rocks from the Sierra de Valle Fértil–La Huerta, Argentina: Petrologic constraints on the origin of igneous rocks in the Ordovician Famatinian–Puna paleoarc. *Journal of South American Earth Sciences* **30**, 29–45.

Otamendi, J. E., Ducea, M. N. & Bergantz, G. W. (2012). Geological, petrological and geochemical evidence for progressive construction of an arc crustal section, Sierra de Valle Fértil, Famatinian Arc, Argentina. *Journal of Petrology* **53**, 761–800.

Pankhurst, R. J., Rapela, C. W., Saavedra, J., Baldo, E., Dahlquist, J., Pascua, I. & Fanning, C. M. (1998). The Famatinian magmatic arc in the central Sierras Pampeanas: an Early to Mid-Ordovician continental arc on the Gondwana margin. In: Pankhurst, R. J. & Rapela, C. W. (eds) *The Proto-Andean Margin of Gondwana. Geological Society, London, Special Publications* **142**, 343–367.

Petterson, M. G., Crawford, M. B. & Windley, B. F. (1993). Petrogenetic implications of neodymium isotope data from the Kohistan batholith, North Pakistan. *Journal of the Geological Society, London* **150**, 125–129.

Pichavant, M. & Macdonald, R. (2007). Crystallization of primitive basaltic magmas at crustal pressures and genesis of the calc-alkaline igneous suite: experimental evidence from St Vincent, Lesser Antilles arc. *Contributions to Mineralogy and Petrology* **154**, 535–558.

Putirka, K. D., Canchola, J., Rash, J., Smith, O., Torrez, G., Paterson, S. R. & Ducea, M. N. (2014). Pluton assembly and the genesis of granitic magmas: Insights from the GIC pluton in cross section, Sierra Nevada Batholith, California. *American Mineralogist* **99**, 1284–1303.

Rapela, C. W., Pankhurst, R. J., Casquet, C., Baldo, E., Saavedra, J. & Galindo, C. (1998). Early evolution of the Proto-Andean margin of South America. *Geology* **26**, 707–710.

Rapp, R. P. (1991). Origin of Archean granitoids and continental evolution. *EOS Transactions, American Geophysical Union* **72**, 225, 229.

Rapp, R. P. & Watson, E. B. (1995). Dehydration melting of metabasalt at 8–32 kbar: implications for continental growth and crust–mantle recycling. *Journal of Petrology* **36**, 891–931.

Ratajeski, K., Sisson, T. & Glazner, A. (2005). Experimental and geochemical evidence for derivation of the El Capitan Granite, California, by partial melting of hydrous gabbroic lower crust. *Contributions to Mineralogy and Petrology* **149**, 713–734.

Reiners, P. W., Nelson, B. K. & Ghiorso, M. S. (1995). Assimilation of felsic crust by basaltic magma: Thermal limits and extents of crustal contamination of mantle-derived magmas. *Geology* **23**, 563–566.

Rioux, M., Hacker, B., Mattinson, J., Kelemen, P., Blusztajn, J. & Gehrels, G. (2007). Magmatic development of an intra-oceanic arc: High-precision U–Pb zircon and whole-rock isotopic analyses from the accreted Talkeetna arc, south–central Alaska. *Geological Society of America Bulletin* **119**, 1168–1184.

Rodriguez-Vargas, A., Koester, E., Mallmann, G., Conceição, R. V., Kawashita, K. & Weber, M. B. I. (2005). Mantle diversity beneath the Colombian Andes, Northern Volcanic Zone: Constraints from Sr and Nd isotopes. *Lithos* **82**, 471–484.

Roeder, P. L. & Emslie, R. F. (1970). Olivine–liquid equilibrium. *Contributions to Mineralogy and Petrology* **29**, 275–289.

Ross, D. C. (1985). Mafic gneissic complex (batholithic root) in the southernmost Sierra Nevada, California. *Geology* **13**, 288–291.

Saito, S., Arima, M., Nakajima, T. & Kimura, J.-I. (2004). Petrogenesis of Ashigawa and Tonogi granitic intrusions, southern part of the Miocene Kofu Granitic Complex, central Japan: M-type granite in the Izu arc collision zone. *Journal of Mineralogical and Petrological Sciences* **99**, 104–117.

Saito, S., Arima, M., Nakajima, T., Misawa, K. & Kimura, J.-I. (2007). Formation of distinct granitic magma batches by partial melting of hybrid lower crust in the Izu arc collision zone, central Japan. *Journal of Petrology* **48**, 1761–1791.

Samson, S. D., Patchett, P. J., Gehrels, G. E. & Anderson, R. G. (1990). Nd and Sr isotopic characterization of the Wrangellia Terrane and implications for crustal growth of the Canadian Cordillera. *Journal of Geology* **98**, 749–762.

Sisson, T. W. & Grove, T. L. (1993). Experimental investigations of the role of H_2O in calc-alkaline differentiation and subduction zone magmatism. *Contributions to Mineralogy and Petrology* **113**, 143–166.

Sisson, T. W., Grove, T. L. & Coleman, D. S. (1996). Hornblende gabbro sill complex at Onion Valley, California, and a mixing origin for the Sierra Nevada batholith. *Contributions to Mineralogy and Petrology* **126**, 81–108.

Sisson, T. W., Ratajeski, K., Hankins, W. B. & Glazner, A. F. (2005). Voluminous granitic magmas from common basaltic sources. *Contributions to Mineralogy and Petrology* **148**, 635–661.

Smith, D. J. (2014). Clinopyroxene precursors to amphibole sponge in arc crust. *Nature Communications* **5** doi:10.1038/ncomms5329.

Smith, I. E. M., Worthington, T. J., Price, R. C., Stewart, R. B. & Maas, R. (2006). Petrogenesis of dacite in an oceanic subduction environment: Raoul Island, Kermadec arc. *Journal of Volcanology and Geothermal Research* **156**, 252–265.

Spandler, C., Arculus, R., Eggins, S., Mavrogenes, J., Price, R. & Reay, A. (2003). Petrogenesis of the Greenhills Complex, Southland, New Zealand: magmatic differentiation and cumulate formation at the roots of a Permian island-arc volcano. *Contributions to Mineralogy and Petrology* **144**, 703–721.

Stern, C. R. (1991). Role of subduction erosion in the generation of Andean magmas. *Geology* **19**, 78–81.

Sun, S. & McDonough, W. F. (1989). Chemical and isotopic systematics of oceanic basalts: implications for mantle composition and processes. In: Saunders, A. D. & Norry, M. J. (eds) *Magmatism in the Ocean Basins. Geological Society, London, Special Publications* **42**, 313–345.

Tepper, J. H., Nelson, B. K., Bergantz, G. W. & Irving, A. J. (1993). Petrology of the Chilliwack Batholith, North Cascades, Washington: Generation of calc-alkaline granitoids by melting of mafic lower crust with variable water fugacity. *Contributions to Mineralogy and Petrology* **113**, 333–351.

Thomas, W. A. & Astini, R. A. (1996). The Argentine Precordillera: a traveller from the Ouachita embayment of North American Laurentia. *Science* **273**, 752–757.

Tibaldi, A. M., Otamendi, J. E., Cristofolini, E. A., Baliani, I., Walker, B. A. & Bergantz, G. W. (2013). Reconstruction of the Early Ordovician Famatinian arc through thermobarometry in lower and middle crustal exposures, Sierra de Valle Fertil, Argentina. *Tectonophysics* **589**, 151–166.

Vernon, R. H., Paterson, S. R. & Geary, E. E. (1989). Evidence for syntectonic intrusion of plutons in the Bear Mountains fault zone, California. *Geology* **17**, 723–726.

Vujovich, G., Godeas, M., Marín, G. & Pezzutti, N. (1996). El complejo magmático de la Sierra de La Huerta, provincia de San Juan. *Actas XIII Congreso Geológico Argentino y III Congreso de Exploración de Hidrocarburos* **3**, 465–475.

Walker, B. A. J., Miller, C. F., Lowery Claiborne, L., Wooden, J. L. & Miller, J. S. (2007). Geology and geochronology of the Spirit Mountain batholith, southern Nevada: Implications for timescales and physical processes of batholith construction. *Journal of Volcanology and Geothermal Research* **167**, 239–262.

Westerman, D. S., Dini, A., Innocenti, F. & Rocchi, S. (2004). Rise and fall of a nested Christmas-tree laccolith complex, Elba Island, Italy. In: Breitkreuz, C. & Petford, N. (eds) *Physical Geology of High-Level Magmatic Systems. Geological Society, London, Special Publications* **234**, 195–213.

Wolf, M. B. & Wyllie, P. J. (1994). Dehydration-melting of amphibolite at 10 kbar: the effects of temperature and time. *Contributions to Mineralogy and Petrology* **115**, 369–383.

Yuan, X., Sobolev, S. V. & Kind, R. (2002). Moho topography in the central Andes and its geodynamic implications. *Earth and Planetary Science Letters* **199**, 389–402.

Zavala, K., Leitch, A. M. & Fisher, G. W. (2011). Silicic segregations of the Ferrar Dolerite Sills, Antarctica. *Journal of Petrology* **52**, 1927–1964.